US008721541B2

US 8,721,541 B2

(54) **PHYSIOLOGICAL MONITOR**

(71) Applicant: **Masimo Corporation**, Irvine, CA (US)

(72) Inventors: **Ammar Al-Ali**, Tustin, CA (US);
Mohamed K. Diab, Ladera Ranch, CA
(US); **Massi E. Kiani**, Laguna Niguel,
CA (US); **Robert James Kopotic**,
Jamul, CA (US); **David Tobler**,
Westminster, CO (US)

(73) Assignee: **Masimo Corporation**, Irvine, CA (US)

(*) Notice: Subject to any disclaimer, the term of this
patent is extended or adjusted under 35
U.S.C. 154(b) by 0 days.

This patent is subject to a terminal dis-
claimer.

(21) Appl. No.: **13/745,590**

(22) Filed: **Jan. 18, 2013**

(65) **Prior Publication Data**

US 2013/0197330 A1 Aug. 1, 2013

Related U.S. Application Data

(63) Continuation of application No. 11/417,931, filed on
May 3, 2006, now Pat. No. 8,364,223, which is a
continuation of application No. 11/104,720, filed on
Apr. 13, 2005, now Pat. No. 7,761,128, which is a
continuation of application No. 10/668,487, filed on
Sep. 22, 2003, now Pat. No. 6,898,452, which is a
continuation of application No. 10/026,013, filed on
Dec. 21, 2001, now Pat. No. 6,714,804, which is a
continuation of application No. 09/323,176, filed on
May 27, 1999, now Pat. No. 6,334,065.

(60) Provisional application No. 60/087,802, filed on Jun.
3, 1998.

(51) **Int. Cl.**
A61B 5/00 (2006.01)
A61B 5/1455 (2006.01)

(52) **U.S. Cl.**
USPC **600/300**; 600/310

(58) **Field of Classification Search**
USPC 600/300, 310, 323, 324
See application file for complete search history.

(56) **References Cited**

U.S. PATENT DOCUMENTS

3,704,706 A 12/1972 Herczfeld et al.
3,847,483 A 11/1974 Shaw et al.
(Continued)

FOREIGN PATENT DOCUMENTS

EP 0 555 553 A2 8/1993
EP 0 807 402 A1 11/1997
WO WO 96/012435 2/1996

OTHER PUBLICATIONS

Confidential Declaration of Michelle Armond in Support of
MASIMO Corporation's Responsive Claim Construction Brief,
MASIMO Corporation v. *Philips Electronics North America Corpo-
ration and Philips Medizin Systeme Böblingen GMBH*, (District of
Delaware, Case No. 1:09-cv-00080 (LPS/MPT) dated Nov. 19, 2010
(Redacted).

(Continued)

Primary Examiner — Eric Winakur
Assistant Examiner — Etsub Berhanu
(74) *Attorney, Agent, or Firm* — Knobbe, Martens, Olson &
Bear, LLP

(57) **ABSTRACT**

A patient monitor has multiple sensors adapted to attach to
tissue sites of a living subject. The sensors generate sensor
signals that are responsive to at least two wavelengths of
optical radiation after attenuation by pulsatile blood within
the tissue sites.

17 Claims, 25 Drawing Sheets
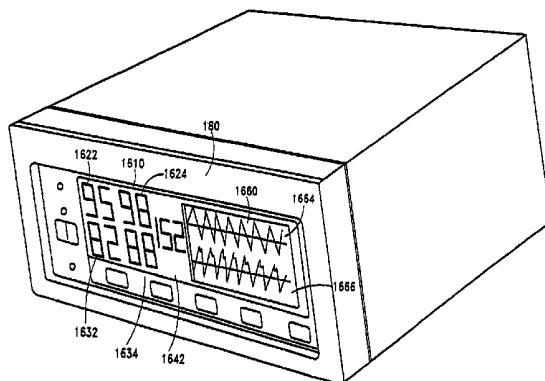
(56)   **References Cited**

U.S. PATENT DOCUMENTS

4,051,522 A	9/1977	Healy et al.
4,109,643 A	8/1978	Bond et al.
4,854,699 A	8/1989	Edgar, Jr.
4,869,253 A	9/1989	Craig, Jr. et al.
4,911,167 A	3/1990	Corenman et al.
4,927,264 A	5/1990	Shiga et al.
4,960,128 A	10/1990	Gordon et al.
4,964,408 A	10/1990	Hink et al.
5,020,516 A	6/1991	Biondi et al.
5,041,187 A	8/1991	Hink et al.
5,069,213 A	12/1991	Polczynski
5,078,136 A	1/1992	Stone et al.
5,163,438 A	11/1992	Gordon et al.
5,218,962 A	6/1993	Mannheimer et al.
5,251,632 A	10/1993	Delpy
5,253,645 A	10/1993	Friedman et al.
5,273,036 A	12/1993	Kronberg et al.
5,308,919 A	5/1994	Minnich
5,319,355 A	6/1994	Russek
5,337,744 A	8/1994	Branigan
5,341,805 A	8/1994	Stavridi et al.
D353,195 S	12/1994	Savage et al.
D353,196 S	12/1994	Savage et al.
5,377,676 A	1/1995	Vari et al.
5,385,144 A	1/1995	Yamanishi et al.
5,396,893 A	3/1995	Oberg et al.
D359,546 S	6/1995	Savage et al.
5,431,170 A	7/1995	Mathews
D361,840 S	8/1995	Savage et al.
D362,063 S	9/1995	Savage et al.
5,448,999 A *	9/1995	Teare et al. 600/546
5,452,717 A	9/1995	Branigan et al.
D363,120 S	10/1995	Savage et al.
5,456,252 A	10/1995	Vari et al.
5,479,934 A	1/1996	Imran
5,482,036 A	1/1996	Diab et al.
5,490,505 A	2/1996	Diab et al.
5,494,043 A	2/1996	O'Sullivan et al.
5,522,388 A	6/1996	Ishikawa et al.
5,533,511 A	7/1996	Kaspari et al.
5,534,851 A	7/1996	Russek
5,542,421 A	8/1996	Erdman
5,561,275 A	10/1996	Savage et al.
5,562,002 A	10/1996	Lalin
5,575,284 A	11/1996	Athan et al.
5,590,649 A	1/1997	Caro et al.
5,602,924 A	2/1997	Durand et al.
5,632,272 A	5/1997	Diab et al.
5,638,816 A	6/1997	Kiani-Azarbayjany et al.
5,638,818 A	6/1997	Diab et al.
5,645,440 A	7/1997	Tobler et al.
5,647,359 A	7/1997	Kohno et al.
5,682,877 A	11/1997	Mondry
5,685,299 A	11/1997	Diab et al.
D393,830 S	4/1998	Tobler et al.
5,743,261 A	4/1998	Mainiero et al.
5,743,262 A	4/1998	Lepper, Jr. et al.
5,743,857 A	4/1998	Shinoda et al.
5,758,644 A	6/1998	Diab et al.
5,760,910 A	6/1998	Lepper, Jr. et al.
5,769,785 A	6/1998	Diab et al.
5,782,757 A	7/1998	Diab et al.
5,785,659 A	7/1998	Caro et al.
5,791,347 A	8/1998	Flaherty et al.
5,810,734 A	9/1998	Caro et al.
5,823,950 A	10/1998	Diab et al.
5,827,181 A	10/1998	Dias et al.
5,830,131 A	11/1998	Caro et al.
5,830,135 A	11/1998	Bosque et al.
5,833,618 A	11/1998	Caro et al.
5,842,979 A	12/1998	Jarman
5,846,190 A	12/1998	Woehrle
5,860,919 A	1/1999	Kiani-Azarbayjany et al.
5,876,335 A *	3/1999	Handy et al. 600/304
5,890,929 A	4/1999	Mills et al.
5,904,654 A	5/1999	Wohltmann et al.
5,919,134 A	7/1999	Diab
5,934,925 A	8/1999	Tobler et al.
5,940,182 A	8/1999	Lepper, Jr. et al.
5,954,053 A	9/1999	Chance et al.
5,995,855 A	11/1999	Kiani et al.
5,997,343 A	12/1999	Mills et al.
6,002,952 A	12/1999	Diab et al.
6,011,986 A	1/2000	Diab et al.
6,027,452 A	2/2000	Flaherty et al.
6,036,642 A	3/2000	Diab et al.
6,045,509 A	4/2000	Caro et al.
6,067,462 A	5/2000	Diab et al.
6,081,735 A	6/2000	Diab et al.
6,088,607 A	7/2000	Diab et al.
6,094,592 A	7/2000	Yorkey et al.
6,110,522 A	8/2000	Lepper, Jr. et al.
6,122,535 A	9/2000	Kaestle et al.
6,124,597 A	9/2000	Shehada
6,128,521 A	10/2000	Marro et al.
6,129,675 A	10/2000	Jay
6,144,868 A	11/2000	Parker
6,151,516 A	11/2000	Kiani-Azarbayjany et al.
6,152,754 A	11/2000	Gerhardt et al.
6,157,850 A	12/2000	Diab et al.
6,165,005 A	12/2000	Mills et al.
6,184,521 B1	2/2001	Coffin, IV et al.
6,206,830 B1	3/2001	Diab et al.
6,229,856 B1	5/2001	Diab et al.
6,232,609 B1	5/2001	Snyder et al.
6,236,872 B1	5/2001	Diab et al.
6,241,683 B1	6/2001	Macklem et al.
6,253,097 B1	6/2001	Aronow et al.
6,256,523 B1	7/2001	Diab et al.
6,263,222 B1	7/2001	Diab et al.
6,278,522 B1	8/2001	Lepper, Jr. et al.
6,280,213 B1	8/2001	Tobler et al.
6,285,896 B1	9/2001	Tobler et al.
6,301,493 B1	10/2001	Marro et al.
6,317,627 B1	11/2001	Ennen et al.
6,321,100 B1	11/2001	Parker
6,325,761 B1	12/2001	Jay
6,334,065 B1	12/2001	Al-Ali et al.
6,343,224 B1	1/2002	Parker
6,349,228 B1	2/2002	Kiani et al.
6,360,114 B1	3/2002	Diab et al.
6,368,283 B1	4/2002	Xu et al.
6,371,921 B1	4/2002	Caro et al.
6,377,829 B1	4/2002	Al-Ali
6,388,240 B2	5/2002	Schulz et al.
6,397,091 B2	5/2002	Diab et al.
6,430,437 B1	8/2002	Marro
6,430,525 B1	8/2002	Weber et al.
6,463,311 B1	10/2002	Diab
6,470,199 B1	10/2002	Kopotic et al.
6,501,975 B2	12/2002	Diab et al.
6,505,059 B1	1/2003	Kollias et al.
6,515,273 B2	2/2003	Al-Ali
6,519,487 B1	2/2003	Parker
6,525,386 B1	2/2003	Mills et al.
6,526,300 B1	2/2003	Kiani et al.
6,541,756 B2	4/2003	Schulz et al.
6,542,764 B1	4/2003	Al-Ali et al.
6,580,086 B1	6/2003	Schulz et al.
6,584,336 B1	6/2003	Ali et al.
6,595,316 B2	7/2003	Cybulski et al.
6,597,932 B2	7/2003	Tian et al.
6,597,933 B2	7/2003	Kiani et al.
6,606,511 B1	8/2003	Ali et al.
6,632,181 B2	10/2003	Flaherty et al.
6,639,668 B1	10/2003	Trepagnier
6,640,116 B2	10/2003	Diab
6,643,530 B2	11/2003	Diab et al.
6,650,917 B2	11/2003	Diab et al.
6,654,624 B2	11/2003	Diab et al.
6,658,276 B2	12/2003	Kiani et al.
6,661,161 B1	12/2003	Lanzo et al.
6,671,531 B2	12/2003	Al-Ali et al.
6,678,543 B2	1/2004	Diab et al.

(56)   References Cited

U.S. PATENT DOCUMENTS

6,684,090	B2	1/2004	Ali et al.
6,684,091	B2	1/2004	Parker
6,697,656	B1	2/2004	Al-Ali
6,697,657	B1	2/2004	Shehada et al.
6,697,658	B2	2/2004	Al-Ali
RE38,476	E	3/2004	Diab et al.
6,699,194	B1	3/2004	Diab et al.
6,714,804	B2	3/2004	Al-Ali et al.
RE38,492	E	4/2004	Diab et al.
6,721,582	B2	4/2004	Trepagnier et al.
6,721,585	B1	4/2004	Parker
6,725,075	B2	4/2004	Al-Ali
6,728,560	B2	4/2004	Kollias et al.
6,735,459	B2	5/2004	Parker
6,745,060	B2	6/2004	Diab et al.
6,760,607	B2	7/2004	Al-Ali
6,770,028	B1	8/2004	Ali et al.
6,771,994	B2	8/2004	Kiani et al.
6,792,300	B1	9/2004	Diab et al.
6,813,511	B2	11/2004	Diab et al.
6,816,741	B2	11/2004	Diab
6,822,564	B2	11/2004	Al-Ali
6,826,419	B2	11/2004	Diab et al.
6,829,501	B2	12/2004	Nielsen
6,830,711	B2	12/2004	Mills et al.
6,850,787	B2	2/2005	Weber et al.
6,850,788	B2	2/2005	Al-Ali
6,852,083	B2	2/2005	Caro et al.
6,861,639	B2	3/2005	Al-Ali
6,898,452	B2	5/2005	Al-Ali et al.
6,920,345	B2	7/2005	Al-Ali et al.
6,931,268	B1	8/2005	Kiani-Azarbayjany et al.
6,934,570	B2	8/2005	Kiani et al.
6,939,305	B2	9/2005	Flaherty et al.
6,943,348	B1	9/2005	Coffin IV
6,950,687	B2	9/2005	Al-Ali
6,961,598	B2	11/2005	Diab
6,970,792	B1	11/2005	Diab
6,979,812	B2	12/2005	Al-Ali
6,985,764	B2	1/2006	Mason et al.
6,993,371	B2	1/2006	Kiani et al.
6,996,427	B2	2/2006	Ali et al.
6,999,904	B2	2/2006	Weber et al.
7,003,338	B2	2/2006	Weber et al.
7,003,339	B2	2/2006	Diab et al.
7,015,451	B2	3/2006	Dalke et al.
7,024,233	B2	4/2006	Ali et al.
7,027,849	B2	4/2006	Al-Ali
7,030,749	B2	4/2006	Al-Ali
7,039,449	B2	5/2006	Al-Ali
7,041,060	B2	5/2006	Flaherty et al.
7,044,918	B2	5/2006	Diab
7,067,893	B2	6/2006	Mills et al.
7,096,052	B2	8/2006	Mason et al.
7,096,054	B2	8/2006	Abdul-Hafiz et al.
7,132,641	B2	11/2006	Schulz et al.
7,142,901	B2	11/2006	Kiani et al.
7,149,561	B2	12/2006	Diab
7,186,966	B2	3/2007	Al-Ali
7,190,261	B2	3/2007	Al-Ali
7,215,984	B2	5/2007	Diab
7,215,986	B2	5/2007	Diab
7,221,971	B2	5/2007	Diab
7,225,006	B2	5/2007	Al-Ali et al.
7,225,007	B2	5/2007	Al-Ali
RE39,672	E	6/2007	Shehada et al.
7,239,905	B2	7/2007	Kiani-Azarbayjany et al.
7,245,953	B1	7/2007	Parker
7,254,429	B2	8/2007	Schurman et al.
7,254,431	B2	8/2007	Al-Ali
7,254,433	B2	8/2007	Diab et al.
7,254,434	B2	8/2007	Schulz et al.
7,272,425	B2	9/2007	Al-Ali
7,274,955	B2	9/2007	Kiani et al.
D554,263	S	10/2007	Al-Ali
7,280,858	B2	10/2007	Al-Ali et al.
7,289,835	B2	10/2007	Mansfield et al.
7,292,883	B2	11/2007	De Felice et al.
7,295,866	B2	11/2007	Al-Ali
7,328,053	B1	2/2008	Diab et al.
7,332,784	B2	2/2008	Mills et al.
7,340,287	B2	3/2008	Mason et al.
7,341,559	B2	3/2008	Schulz et al.
7,343,186	B2	3/2008	Lamego et al.
D566,282	S	4/2008	Al-Ali et al.
7,355,512	B1	4/2008	Al-Ali
7,356,365	B2	4/2008	Schurman
7,371,981	B2	5/2008	Abdul-Hafiz
7,373,193	B2	5/2008	Al-Ali et al.
7,373,194	B2	5/2008	Weber et al.
7,376,453	B1	5/2008	Diab et al.
7,377,794	B2	5/2008	Al-Ali et al.
7,377,899	B2	5/2008	Weber et al.
7,383,070	B2	6/2008	Diab et al.
7,415,297	B2	8/2008	Al-Ali et al.
7,428,432	B2	9/2008	Ali et al.
7,438,683	B2	10/2008	Al-Ali et al.
7,440,787	B2	10/2008	Diab
7,454,240	B2	11/2008	Diab et al.
7,467,002	B2	12/2008	Weber et al.
7,469,157	B2	12/2008	Diab et al.
7,471,969	B2	12/2008	Diab et al.
7,471,971	B2	12/2008	Diab et al.
7,483,729	B2	1/2009	Al-Ali et al.
7,483,730	B2	1/2009	Diab et al.
7,489,958	B2	2/2009	Diab et al.
7,496,391	B2	2/2009	Diab et al.
7,496,393	B2	2/2009	Diab et al.
D587,657	S	3/2009	Al-Ali et al.
7,499,741	B2	3/2009	Diab et al.
7,499,835	B2	3/2009	Weber et al.
7,500,950	B2	3/2009	Al-Ali et al.
7,509,154	B2	3/2009	Diab et al.
7,509,494	B2	3/2009	Al-Ali
7,510,849	B2	3/2009	Schurman et al.
7,526,328	B2	4/2009	Diab et al.
7,530,942	B1	5/2009	Diab
7,530,949	B2	5/2009	Al Ali et al.
7,530,955	B2	5/2009	Diab et al.
7,563,110	B2	7/2009	Al-Ali et al.
7,596,398	B2	9/2009	Al-Ali et al.
7,618,375	B2	11/2009	Flaherty
D606,659	S	12/2009	Kiani et al.
7,647,083	B2	1/2010	Al-Ali et al.
D609,193	S	2/2010	Al-Ali et al.
D614,305	S	4/2010	Al-Ali et al.
RE41,317	E	5/2010	Parker
7,729,733	B2	6/2010	Al-Ali et al.
7,734,320	B2	6/2010	Al-Ali
7,761,127	B2	7/2010	Al-Ali et al.
7,761,128	B2	7/2010	Al-Ali et al.
7,764,982	B2	7/2010	Dalke et al.
D621,516	S	8/2010	Kiani et al.
7,791,155	B2	9/2010	Diab
7,801,581	B2	9/2010	Diab
7,822,452	B2	10/2010	Schurman et al.
RE41,912	E	11/2010	Parker
7,844,313	B2	11/2010	Kiani et al.
7,844,314	B2	11/2010	Al-Ali
7,844,315	B2	11/2010	Al-Ali
7,865,222	B2	1/2011	Weber et al.
7,873,497	B2	1/2011	Weber et al.
7,880,606	B2	2/2011	Al-Ali
7,880,626	B2	2/2011	Al-Ali et al.
7,891,355	B2	2/2011	Al-Ali et al.
7,894,868	B2	2/2011	Al-Ali et al.
7,899,507	B2	3/2011	Al-Ali et al.
7,899,518	B2	3/2011	Trepagnier et al.
7,904,132	B2	3/2011	Weber et al.
7,909,772	B2	3/2011	Popov et al.
7,910,875	B2	3/2011	Al-Ali
7,919,713	B2	4/2011	Al-Ali et al.
7,937,128	B2	5/2011	Al-Ali
7,937,129	B2	5/2011	Mason et al.

(56)   **References Cited**

U.S. PATENT DOCUMENTS

7,937,130	B2	5/2011	Diab et al.
7,941,199	B2	5/2011	Kiani
7,951,086	B2	5/2011	Flaherty et al.
7,957,780	B2	6/2011	Lamego et al.
7,962,188	B2	6/2011	Kiani et al.
7,962,190	B1	6/2011	Diab et al.
7,976,472	B2	7/2011	Kiani
7,988,637	B2	8/2011	Diab
7,990,382	B2	8/2011	Kiani
7,991,446	B2	8/2011	Al-Ali et al.
8,000,761	B2	8/2011	Al-Ali
8,008,088	B2	8/2011	Bellott et al.
RE42,753	E	9/2011	Kiani-Azarbayjany et al.
8,019,400	B2	9/2011	Diab et al.
8,028,701	B2	10/2011	Al-Ali et al.
8,029,765	B2	10/2011	Bellott et al.
8,036,728	B2	10/2011	Diab et al.
8,046,040	B2	10/2011	Ali et al.
8,046,041	B2	10/2011	Diab et al.
8,046,042	B2	10/2011	Diab et al.
8,048,040	B2	11/2011	Kiani
8,050,728	B2	11/2011	Al-Ali et al.
RE43,169	E	2/2012	Parker
8,118,620	B2	2/2012	Al-Ali et al.
8,126,528	B2	2/2012	Diab et al.
8,128,572	B2	3/2012	Diab et al.
8,130,105	B2	3/2012	Al-Ali et al.
8,145,287	B2	3/2012	Diab et al.
8,150,487	B2	4/2012	Diab et al.
8,175,672	B2	5/2012	Parker
8,180,420	B2	5/2012	Diab et al.
8,182,443	B1	5/2012	Kiani
8,185,180	B2	5/2012	Diab et al.
8,190,223	B2	5/2012	Al-Ali et al.
8,190,227	B2	5/2012	Diab et al.
8,203,438	B2	6/2012	Kiani et al.
8,224,411	B2	7/2012	Al-Ali et al.
8,228,181	B2	7/2012	Al-Ali
8,229,533	B2	7/2012	Diab et al.
8,255,026	B1	8/2012	Al-Ali
8,255,028	B2	8/2012	Al-Ali et al.
8,260,577	B2	9/2012	Weber et al.
8,274,360	B2	9/2012	Sampath et al.
8,310,336	B2	11/2012	Muhsin et al.
8,315,683	B2	11/2012	Al-Ali et al.
RE43,860	E	12/2012	Parker
8,337,403	B2	12/2012	Al-Ali et al.
8,346,330	B2	1/2013	Lamego
8,353,842	B2	1/2013	Al-Ali et al.
8,355,766	B2	1/2013	MacNeish, III et al.
8,359,080	B2	1/2013	Diab et al.
8,364,223	B2	1/2013	Al-Ali et al.
8,364,226	B2	1/2013	Diab et al.
8,385,995	B2	2/2013	Al-Ali et al.
8,399,822	B2	3/2013	Al-Ali
8,401,602	B2	3/2013	Kiani
8,405,608	B2	3/2013	Al-Ali et al.
8,414,499	B2	4/2013	Al-Ali et al.
8,418,524	B2	4/2013	Al-Ali
8,423,106	B2	4/2013	Lamego et al.
8,428,967	B2	4/2013	Olsen et al.
8,430,817	B1	4/2013	Al-Ali et al.
8,437,825	B2	5/2013	Dalvi et al.
8,455,290	B2	6/2013	Siskavich
8,457,703	B2	6/2013	Al-Ali
8,457,707	B2	6/2013	Kiani
8,463,349	B2	6/2013	Diab et al.
8,466,286	B2	6/2013	Bellott et al.
8,471,713	B2	6/2013	Poeze et al.
8,473,020	B2	6/2013	Kiani et al.
8,483,787	B2	7/2013	Al-Ali et al.
8,489,364	B2	7/2013	Weber et al.
8,498,684	B2	7/2013	Weber et al.
8,509,867	B2	8/2013	Workman et al.
8,515,509	B2	8/2013	Bruinsma et al.
8,523,781	B2	9/2013	Al-Ali
2004/0054261	A1*	3/2004	Kamataki et al. 600/300

OTHER PUBLICATIONS

Declaration of Perry D. Oldham in Support of MASIMO Corporation's Opening Claim Construction Brief, *MASIMO Corporation* v. *Philips Electronics North America Corporation and Philips Medizin Systeme Böblingen GMBH*, (District of Delaware, Case No. 1:09-cv-00080 (LPS/MPT) dated Oct. 19, 2010.

Declaration of Robert T. Stone in Support of Philips' Responsive Markman Brief, *MASIMO Corporation* v. *Philips Electronics North America Corporation and Philips Medizin Systeme Böblingen GMBH*, (District of Delaware, Case No. 1:09-cv-00080 (LPS/MPT) dated Nov. 15, 2010.

Dudell, Glode, et al., "What Constitutes Adequate Oxygenation?" *Pediatrics*, Jan. 1990, pp. 39-41.

Mallinckrodt inc. v. *Masimo Corp.*, 2004 U.S. Dist. Lexis 28518 (C.D. Cal. Jul. 12, 2004).

Mallinckrodt, Inc. v. *Masimo Corp.*, 147 Fed. Appx. 158, 2005 WL 2139867 (Fed. Cir. 2005).

Mallinckrodt, Inc. v. *Masimo Corp.*, 254 F. Supp.2d 1140 (C.D. Cal. 2003).

Masimo Corporation v. *Philips Electronics North America Corporation and Philips Medizin Systeme Böblingen GMBH*, (District of Delaware, Case No. 09-000080(JJF)) Complaint for Patent Infringement dated Feb. 3, 2009, pp. 1-13.

Masimo Corporation v. *Philips Electronics North America Corporation and Philips Medizin Systeme Böblingen GMBH*, (District of Delaware, Case No. 09-00080(JJF)) First Amended Complaint for Patent Infringement dated May 12, 2009, pp. 1-16.

Masimo Corporation v. *Philips Electronics North America Corporation and Philips Medizin Systeme Böblingen GMBH*, (District of Delaware, Case No. 09-00080(JJF)) Defendants' Answer and Philips Electronics North America Corporation's Counterclaims to Masimo's First Amended Complaint dated Jun. 15, 2009, pp. 1-65.

Masimo Corporation v. *Philips Electronics North America Corporation and Philips Medizin Systeme Böblingen GMBH*, (District of Delaware, Case No. 09-00080(JJF)) Masimo's Answer to Philips' Counterclaims dated Jul. 9, 2009, pp. 1-68.

Masimo Corporation v. *Philips Electronics North America Corporation and Philips Medizin Systeme Böblingen GMBH*, (District of Delaware, Case No. 09-00080(JJF)) Defendant/Counterclaim-Plaintiff Philips Electronics North America Corporation Answer to Masimo's Counterclaims dated Aug. 3, 2009, pp. 1-23.

Masimo Corporation v. *Philips Electronics North America Corporation and Philips Medizin Systeme Böblingen GMBH*, (District of Delaware, Case No. 09-00080(JJF)) Defendants' Answer and Philips Electronics North America Corporation's Amended Counterclaims to Masimo's First Amended Complaint, dated Apr. 21, 2010, pp. 1-62.

Masimo Corporation v. *Philips Electronics North America Corporation and Philips Medizin Systeme Böblingen GMBH*, (District of Delaware, Case No. 09-00080(JJF)) Masimo's Answer to Philips' Amended Counterclaims, dated May 10, 2010, pp. 1-76.

Masimo Corporation v. *Philips Electronics North America Corporation and Philips Medizin Systeme Böblingen GMBH*, (District of Delaware, Case No. 09-00080(JJF)) Philips Electronics North America Corporation's Answer to Masimo's Amended Counterclaims (D.I. 102) dated May 27, 2010, pp. 1-24.

Masimo Corporation v. *Philips Electronics North America Corporation and Philips Medizin Systeme Böblingen GMBH*, (District of Delaware, Case No. 09-00080(JJF)) Philips North America Corporation and Philips Medizin Systeme Boblingen GMBH's Seventh Supplemental Objections and Responses to Masimo Corporation's First Set of Interrogatories (Nos. 1-8) dated Jun. 30, 2010, pp. 1-40 (redacted).

MASIMO Corporation's Opening Claim Construction Brief, *MASIMO Corporation* v. *Philips Electronics North America Corporation and Philips Medizin Systeme Böblingen GMBH*, (District of Delaware, Case No. 1:09-cv-00080 (LPS/MPT) dated Oct. 19, 2010.

(56) **References Cited**

OTHER PUBLICATIONS

MASIMO Corporation's Responsive Claim Construction Brief, *MASIMO Corporation v. Philips Electronics North America Corporation and Philips Medizin Systeme Böblingen GMBH*, (District of Delaware, Case No. 1:09-cv-00080 (LPS/MPT) dated Nov. 19, 2010 (Redacted).

MASIMO's Technical Tutorial, *MASIMO Corporation v. Philips Electronics North America Corporation and Philips Medizin Systeme Böblingen GMBH*, (District of Delaware, Case No. 1:09-cv-00080 (LPS/MPT) dated Dec. 1, 2010.

Murray, Willie et al., "The Peripheral Pulse Wave: Information Overlooked", *Journal of Clinical Monitoring*, vol. 12, pp. 365-377, Sep. 1996.

Neuhof, H. et al., "Simultaneous Continuous Measurement of Arterial and Mixed Venous Partial O2 Saturation", The Oxygen Status of Arterial Blood, Zander, Mertzlufft (eds.), pp. 273-278 (Karger, Basel 1991).

Philips' Opening Markman Brief, *MASIMO Corporation v. Philips Electronics North America Corporation and Philips Medizin Systeme Böblingen GMBH*, (District of Delaware, Case No. 1:09-cv00080 (LPS/MPT) dated Oct. 19, 2010.

Philips' Responsive Markman Brief, *MASIMO Corporation v. Philips Electronics North America Corporation and Philips Medizin Systeme Böblingen GMBH*, (District of Delaware, Case No. 1:09-cv00080 (LPS/MPT) dated Nov. 22, 2010.

Phlips' Claim Construction Hearing, Presentation Materials, *MASIMO Corporation v. Philips Electronics North America Corpo-*

ration and Philips Medizin Systeme Böblingen GMBH, (District of Delaware, Case No. 1:09-cv-00080 (LPS/MPT) dated Dec. 1, 2010.

Report and Recommendation re Claim Construction, *MASIMO Corporation v. Philips Electronics North America Corporation and Philips Medizin Systeme Böblingen GMBH*, (District of Delaware, Case No. 1:09-cv-00080 (LPS/MPT) dated Feb. 18, 2011.

Revised Joint Claim Construction Chart, *MASIMO Corporation v. Philips Electronics North America Corporation and Philips Medizin Systeme Böblingen GMBH*, (District of Delaware, Case No. 1:09-cv-00080 (LPS/MPT) dated Oct. 19, 2010.

Search Report received for European Patent Application No. 99 925 958.3, dated Mar. 20, 2009 in 4 pages.

Steinke, John M., Comparison of Mie Theory and the Light Scattering of Red Blood Cells:, *Applied Optics*, vol. 27, No. 19, Oct. 1, 1998, pp. 4027-4033.

Transcript of Markman Hearing, *MASIMO Corporation v. Philips Electronics North America Corporation and Philips Medizin Systeme Böblingen GMBH*, (District of Delaware, Case No. 1:09-cv-00080 (LPS/MPT) dated Dec. 1, 2010.

Vjayakumar, E., et al., "Pulse Oximetry in Infants of <1500 gm Birth Weight on Supplemental Oxygen: A national Survey", Journal of Perinatology, vol. 17, No. 5, 1997, pp. 341-345.

White, Katherine, "Completing the Hemodynamic Picture: Sv_{ox}", *Heart & Lung*, May 1985, vol. 14, No. 3.

Wolf, Martin, et al., "Continuous Noninvasive Measurement of Cerebral Arterial and Venous Oxygen Saturation at the Bedside in Mechanically Ventilated Noenates\", *Critl Care Med*, 1997, vol. 25, No. 9, pp. 1579-1582.
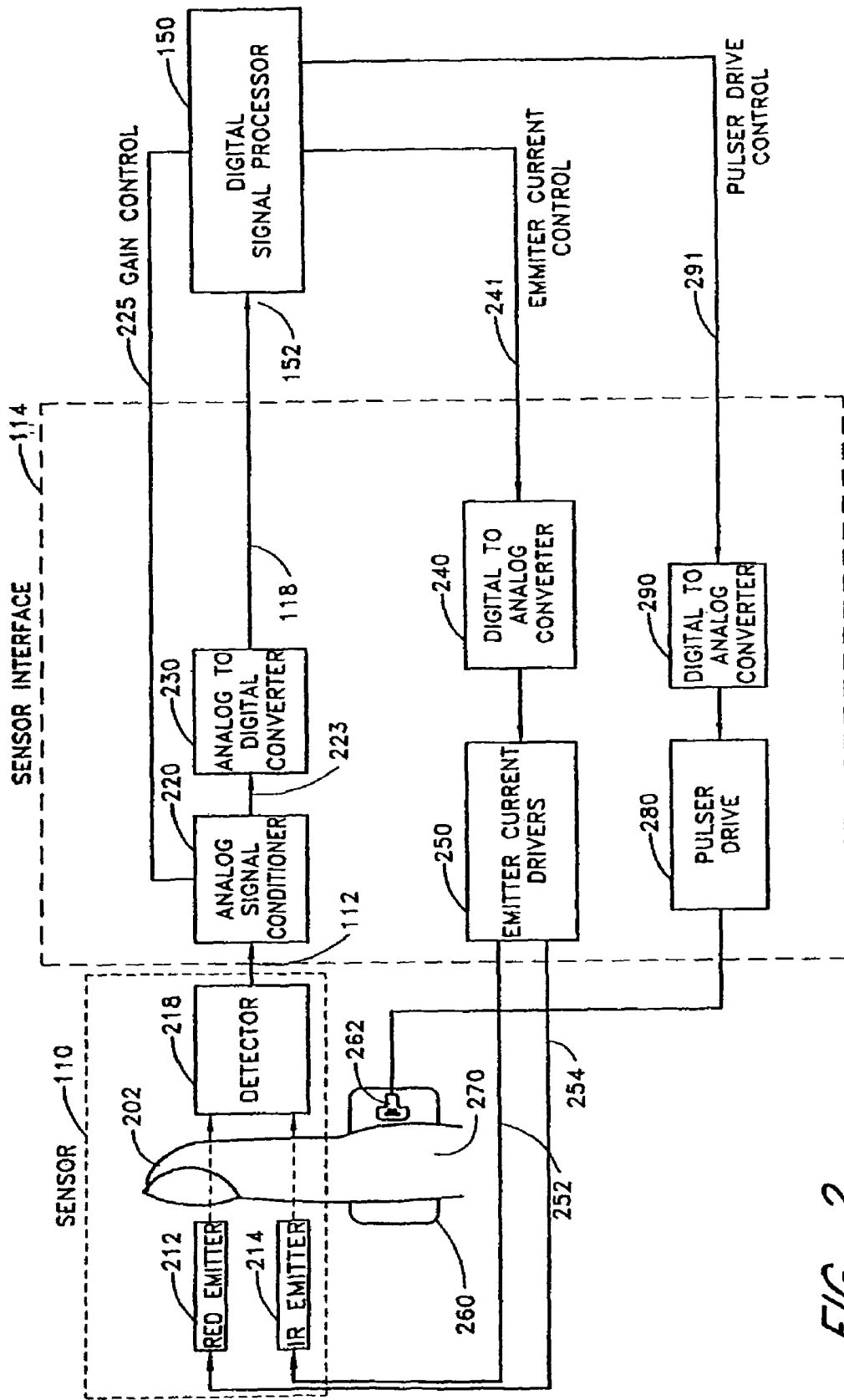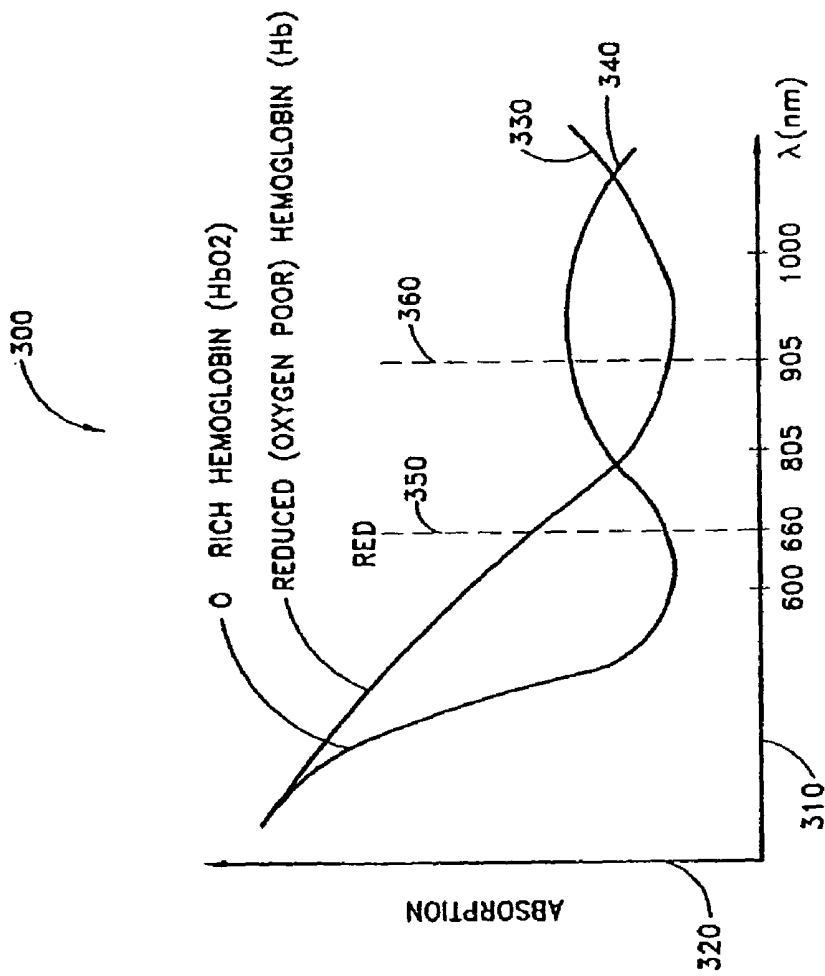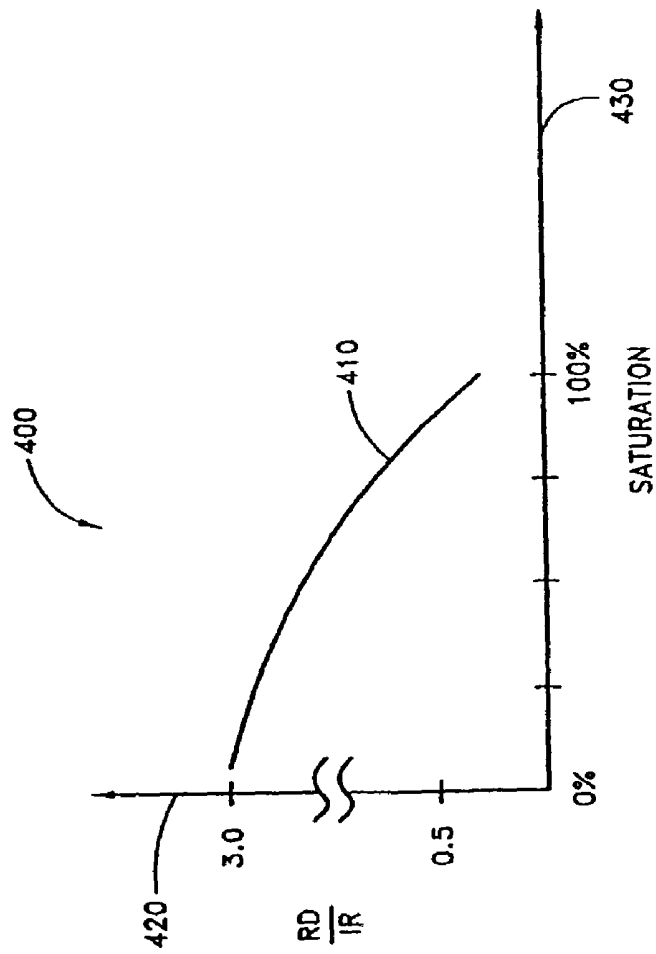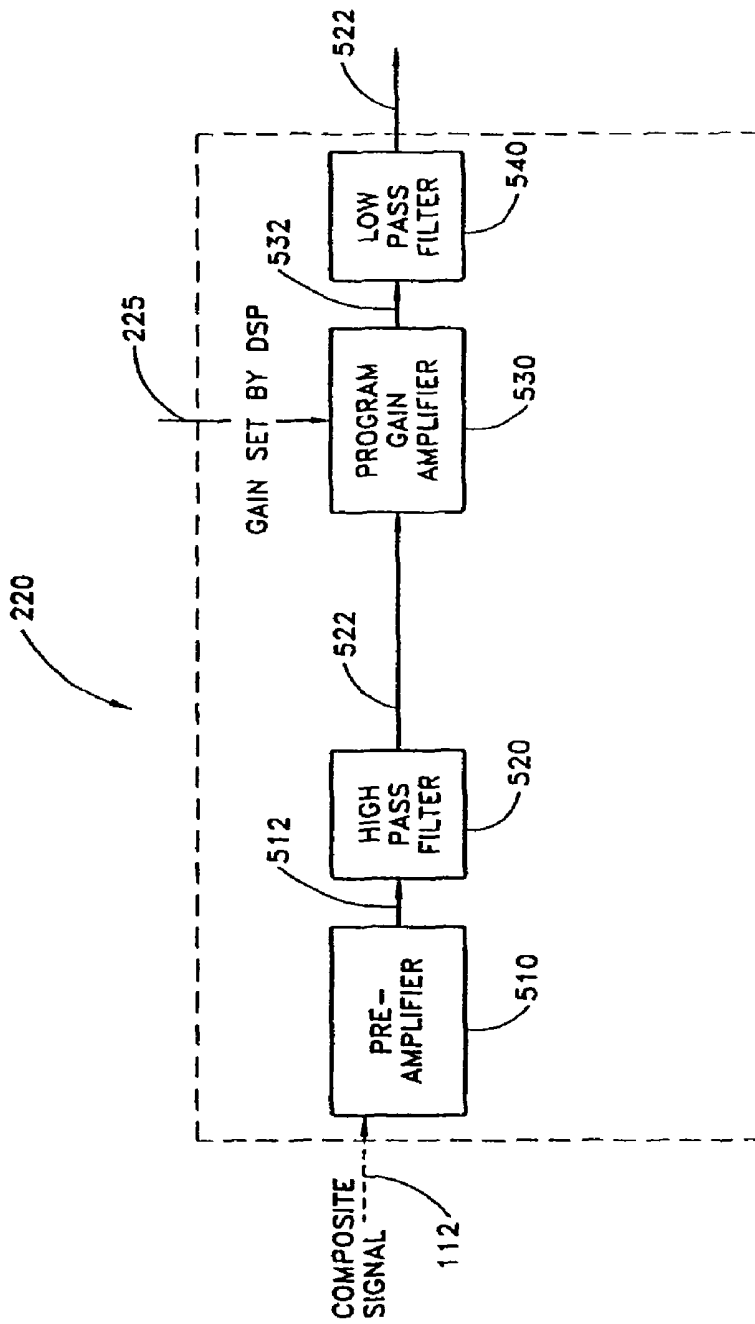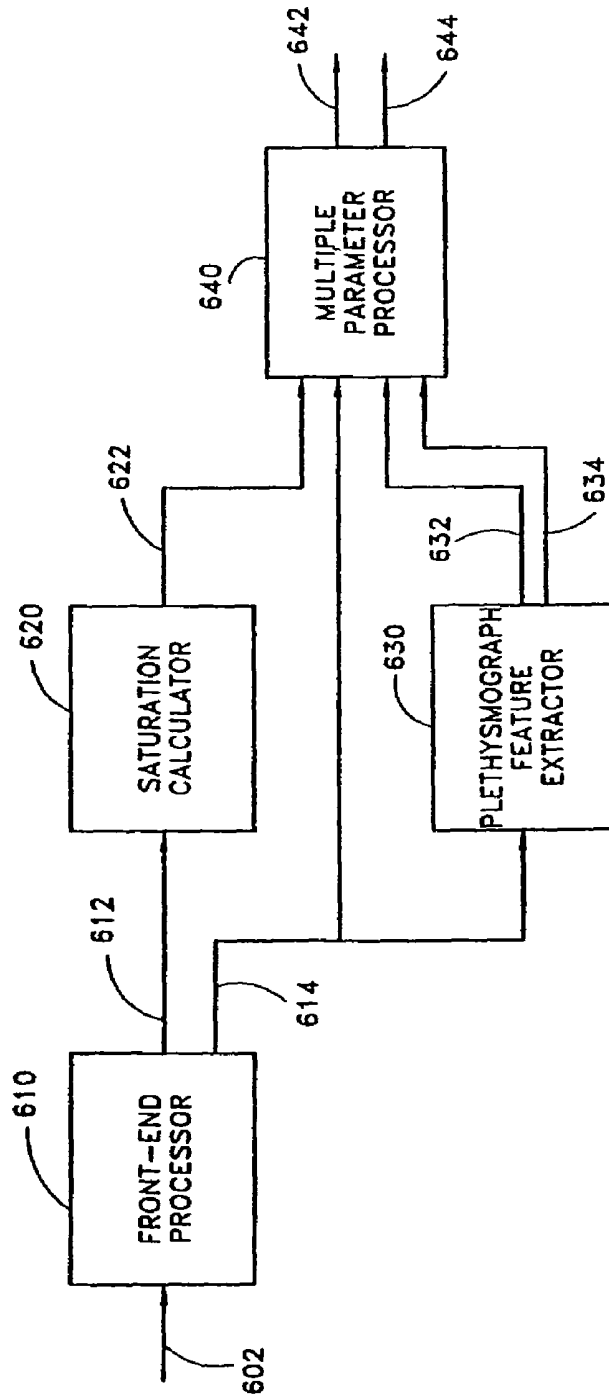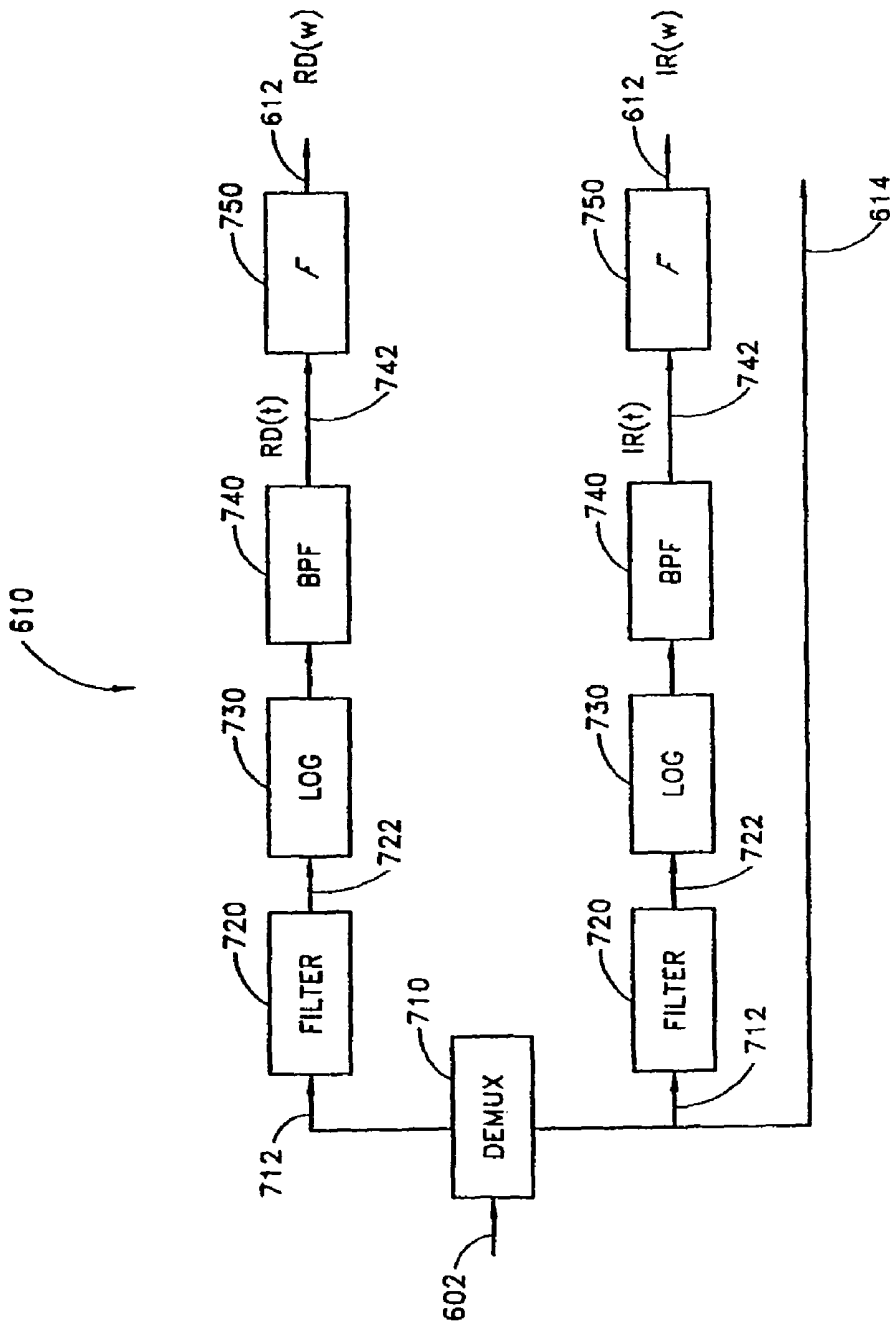
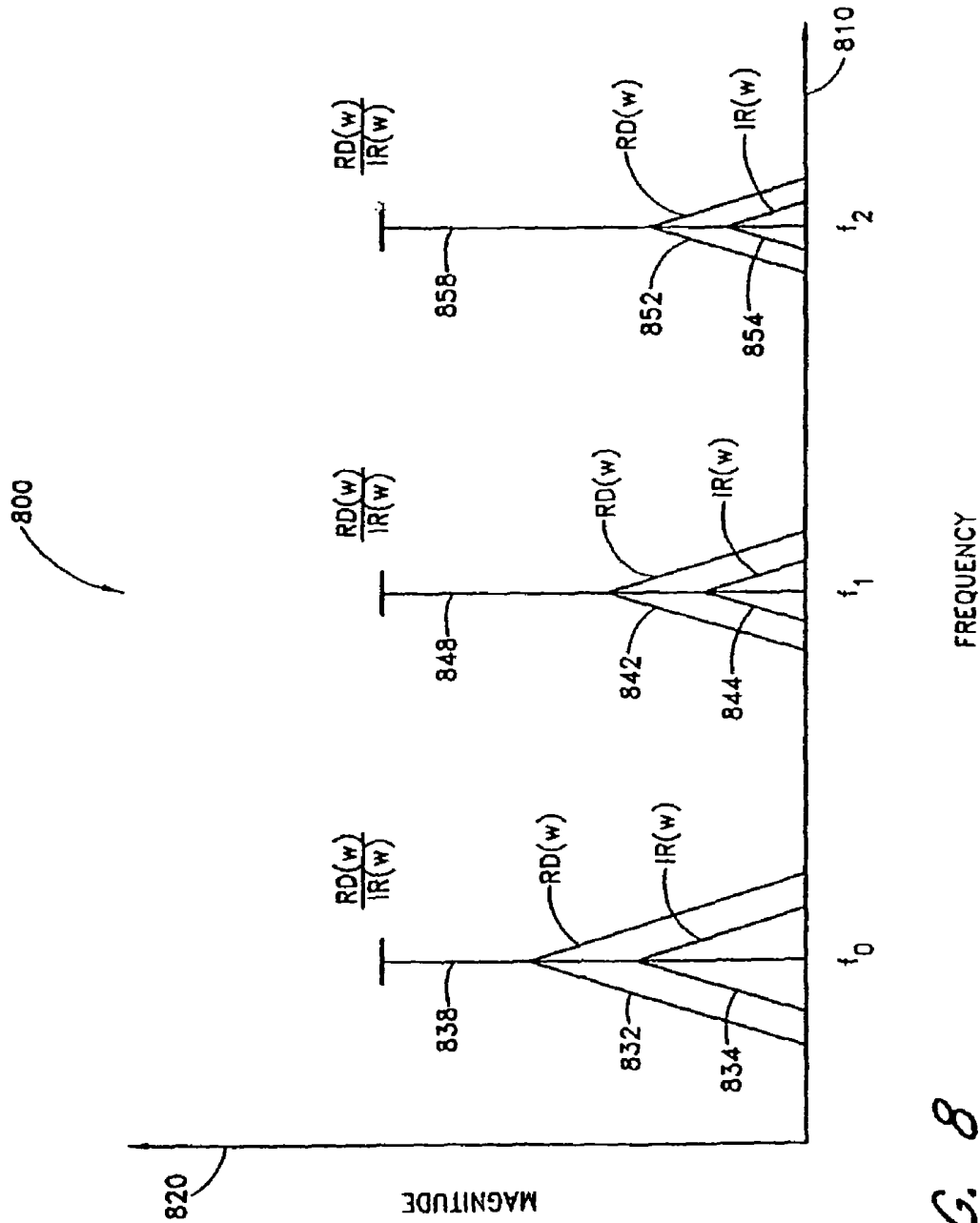* cited by examiner

FIG. 1A
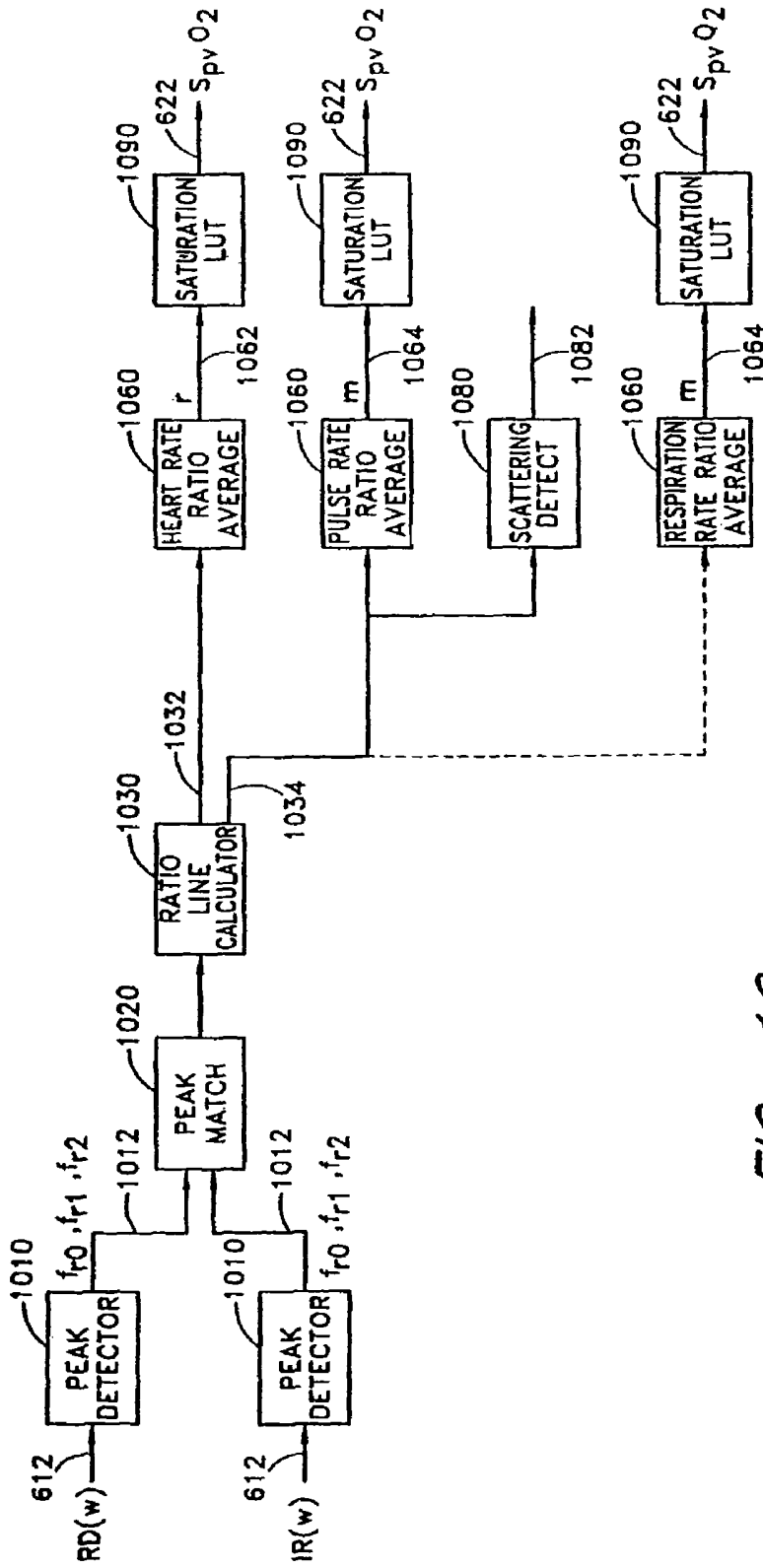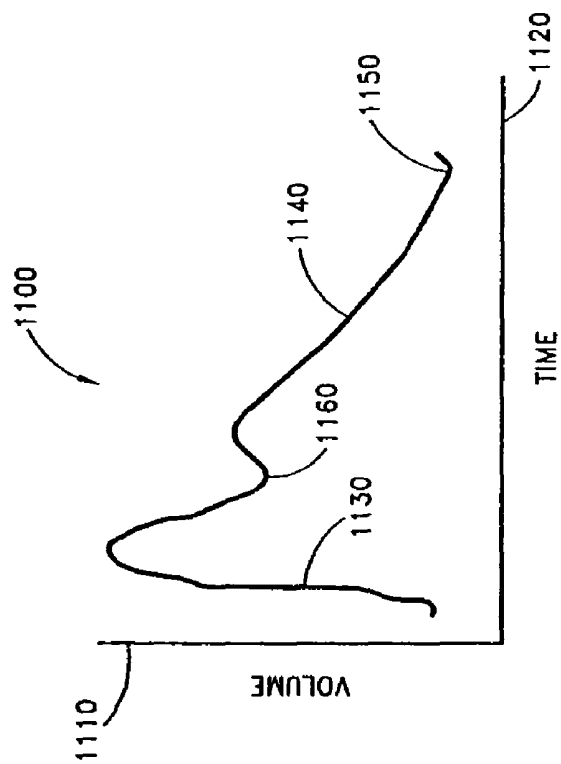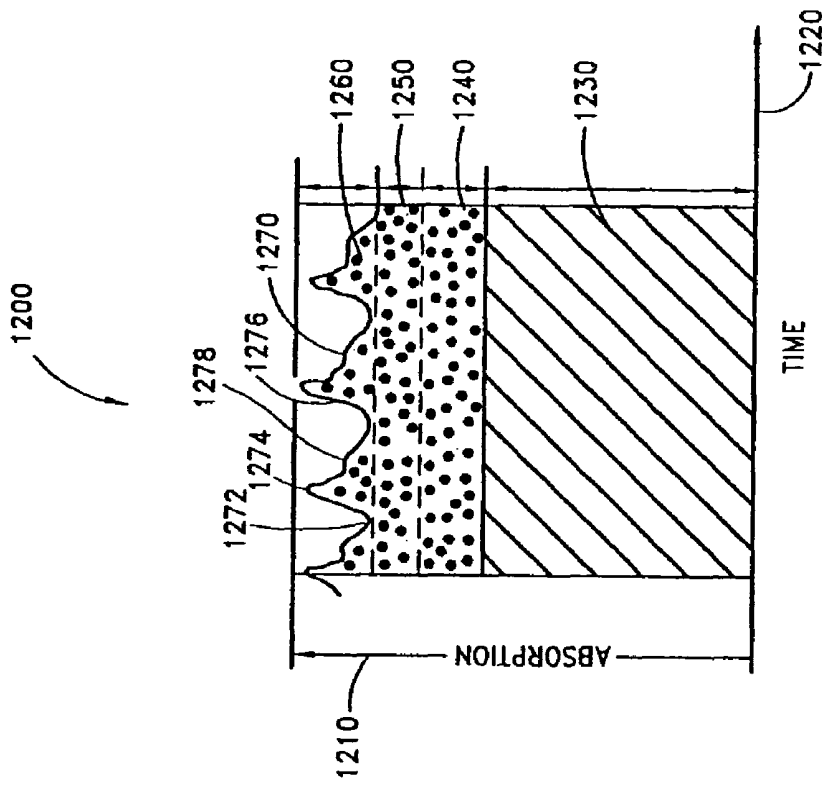
FIG. 1B
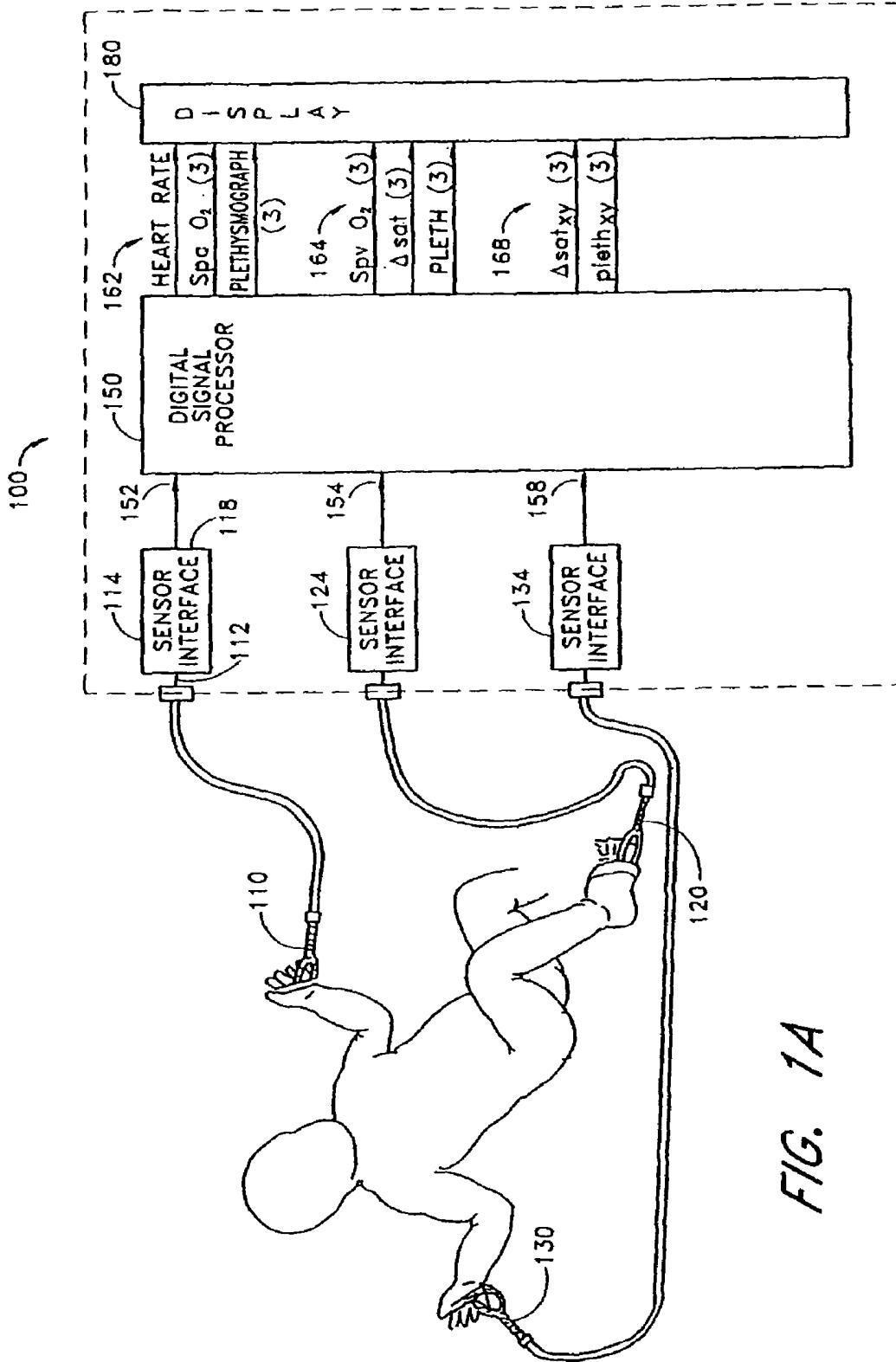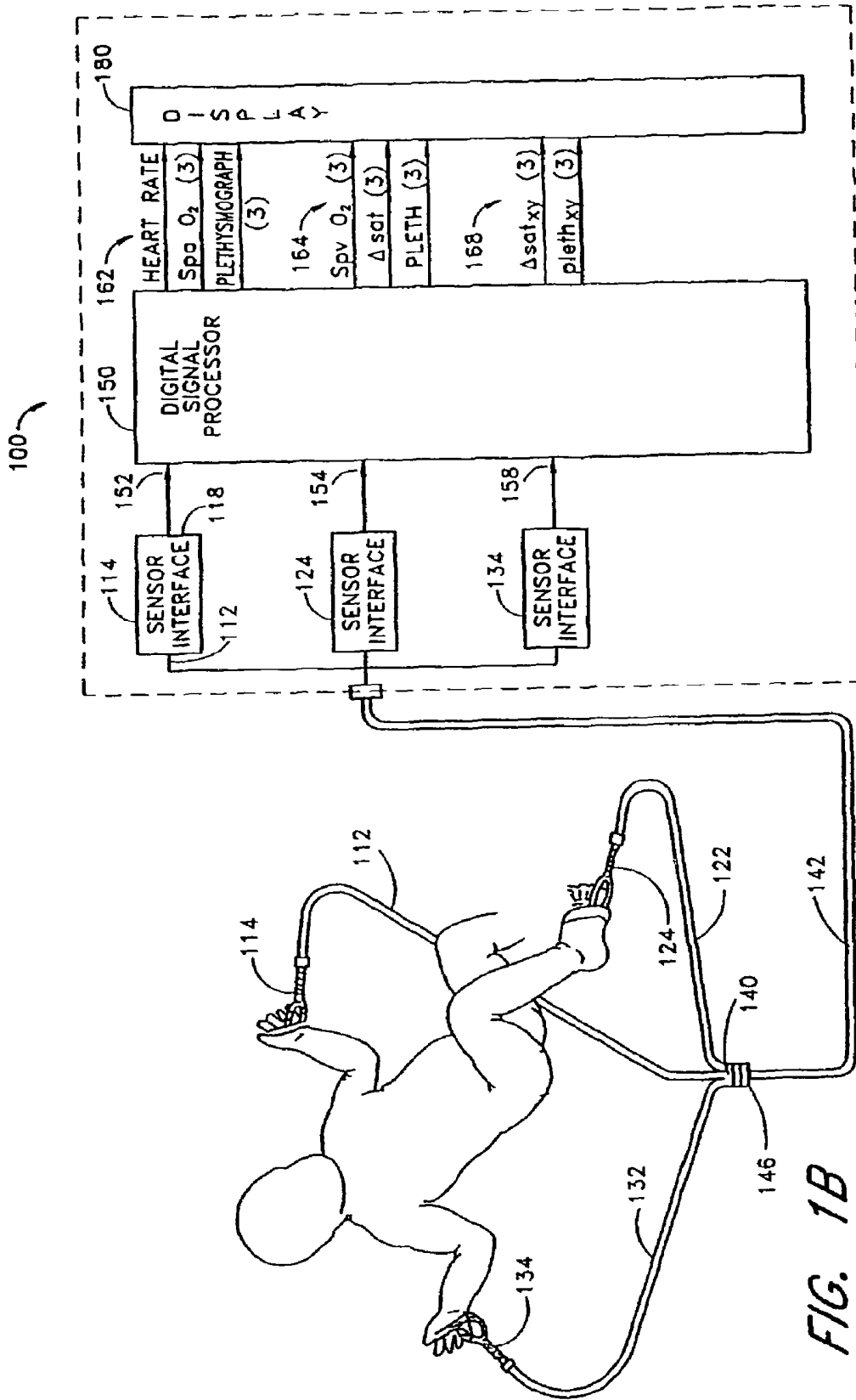
FIG. 2

FIG. 3

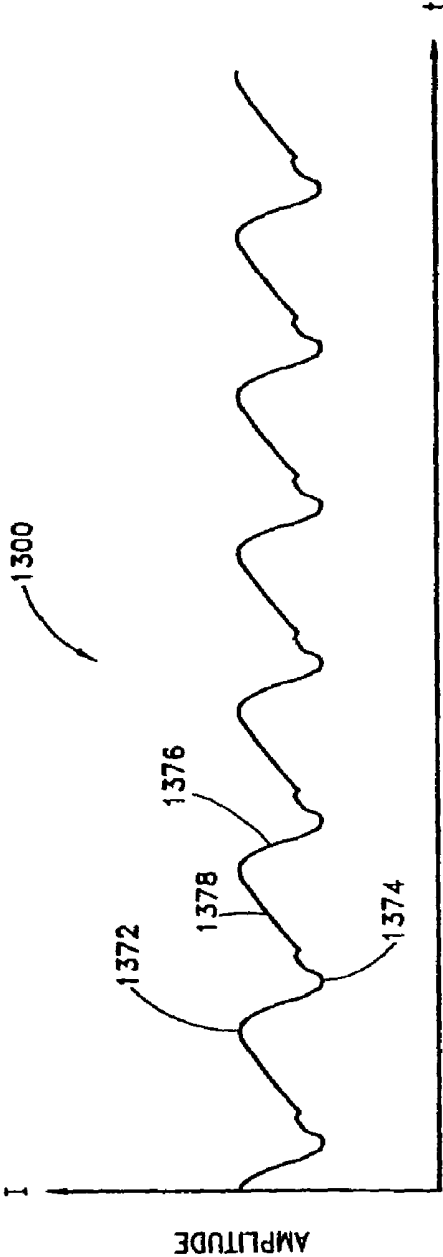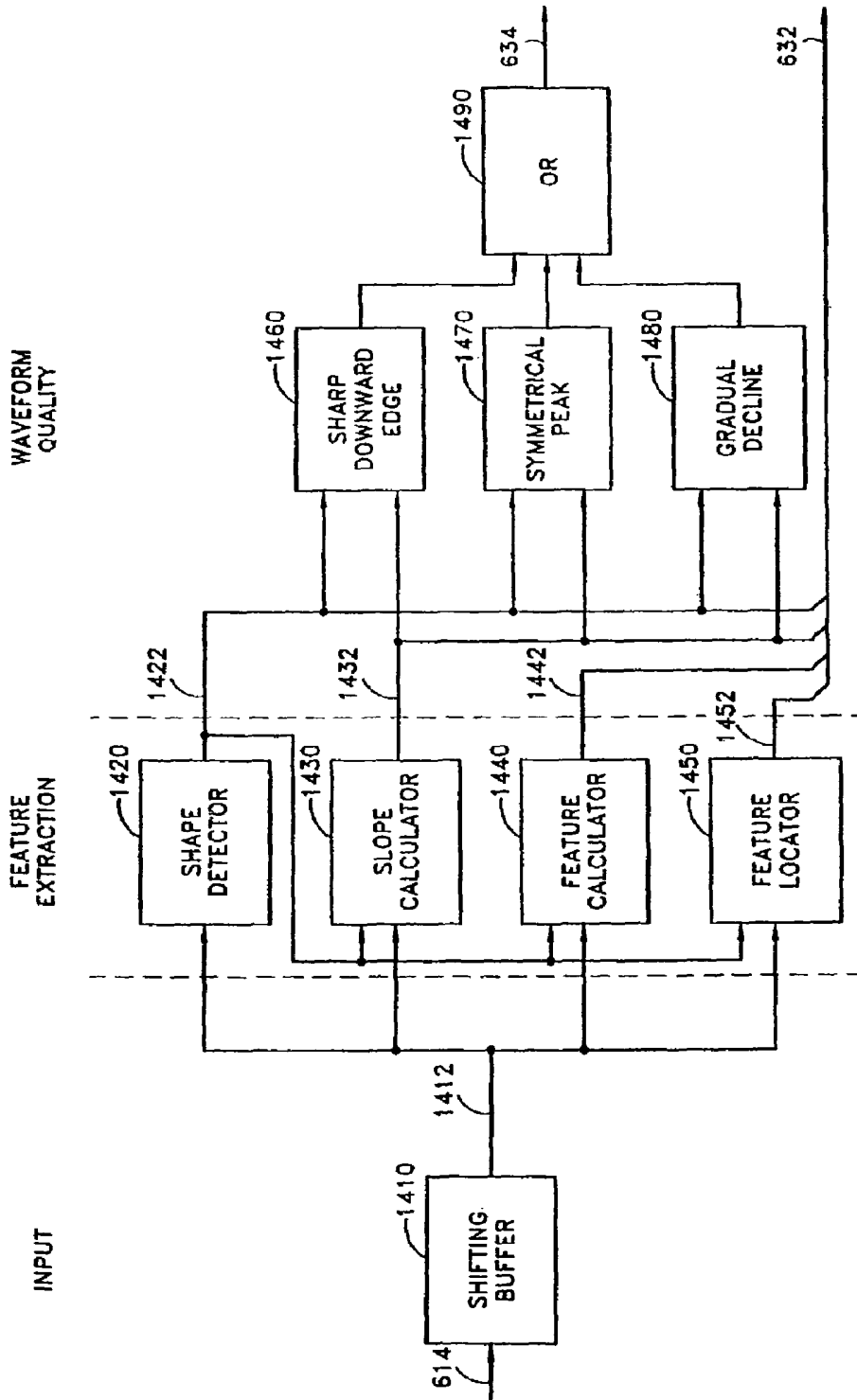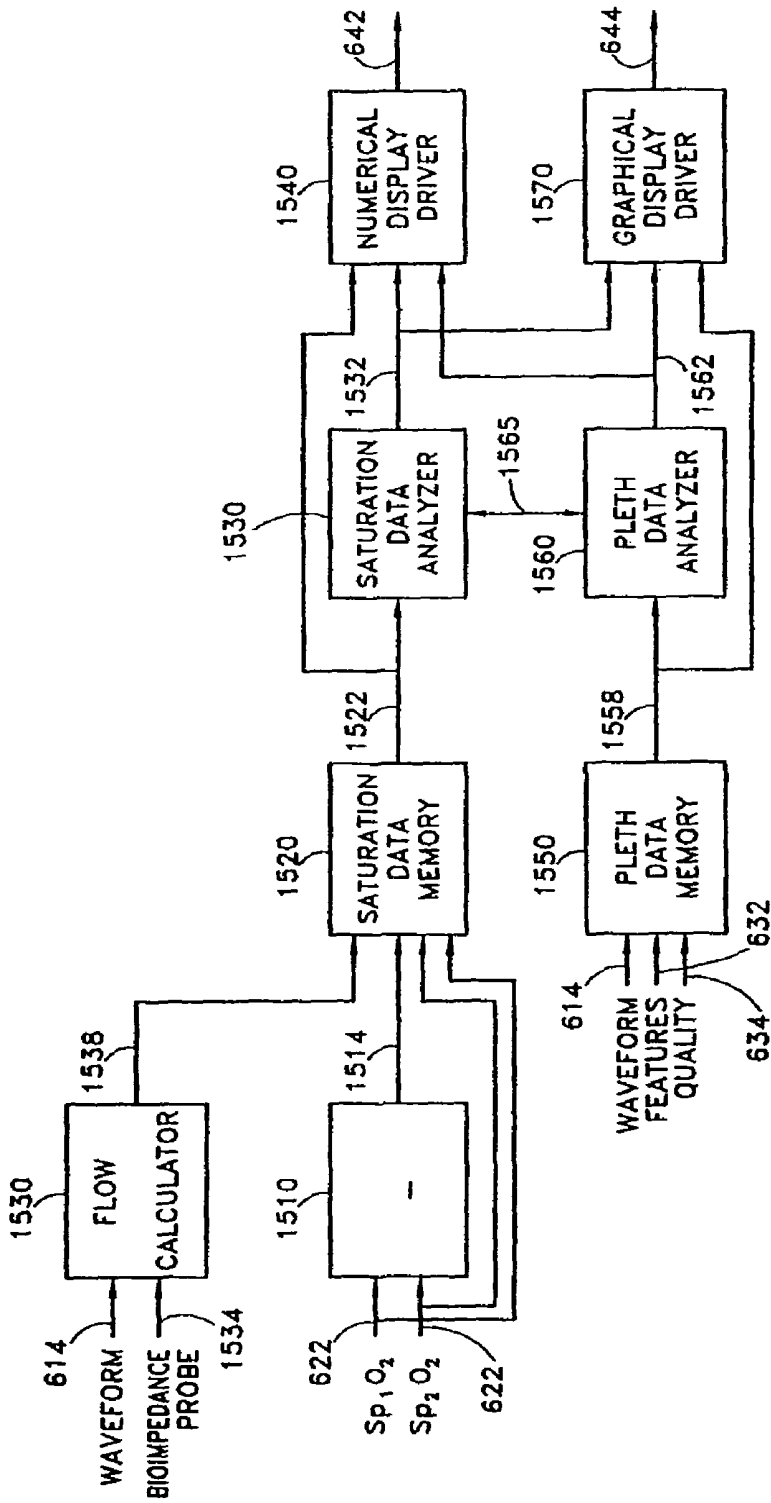*FIG. 4*

FIG. 5

FIG. 6

FIG. 7
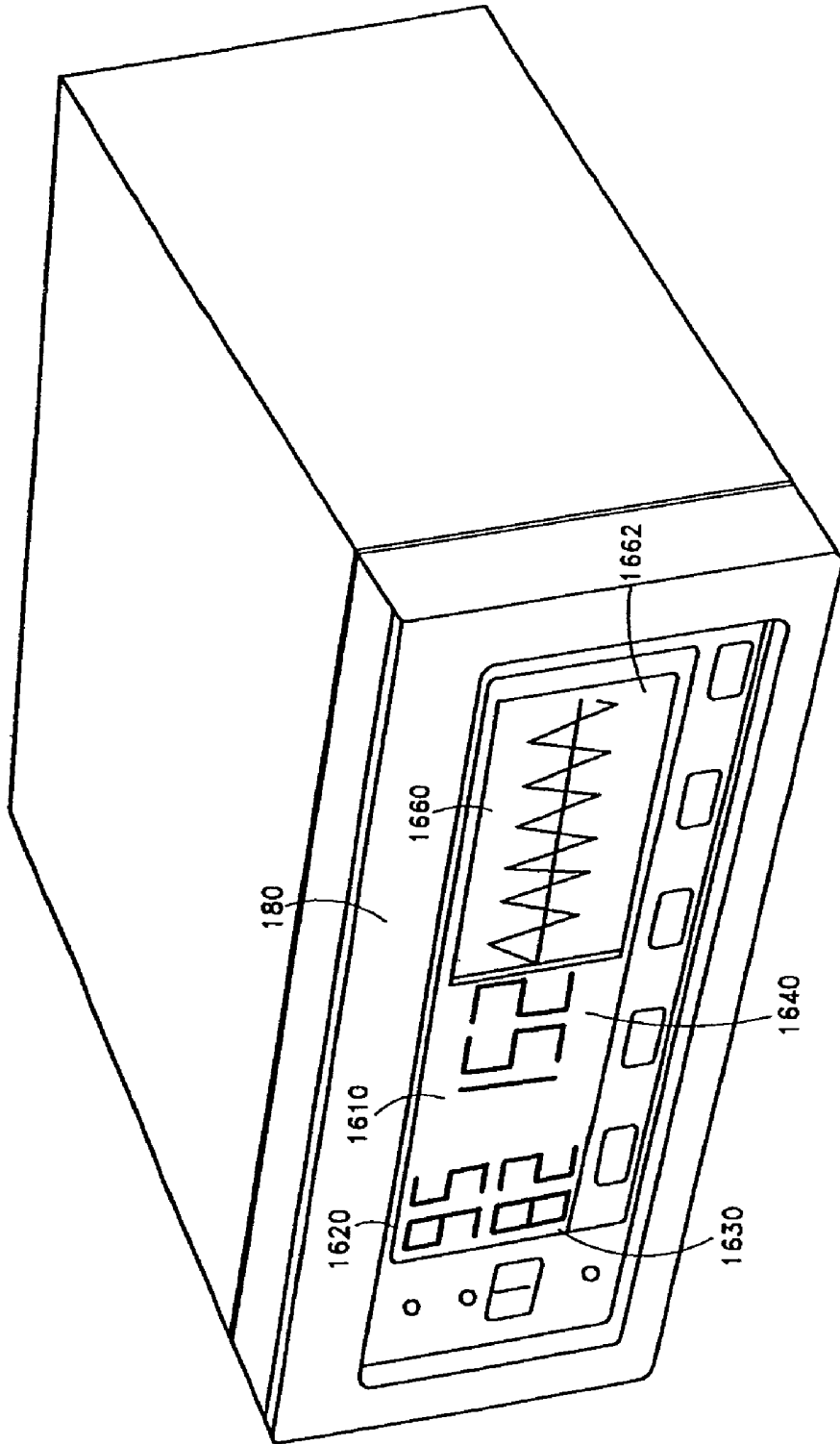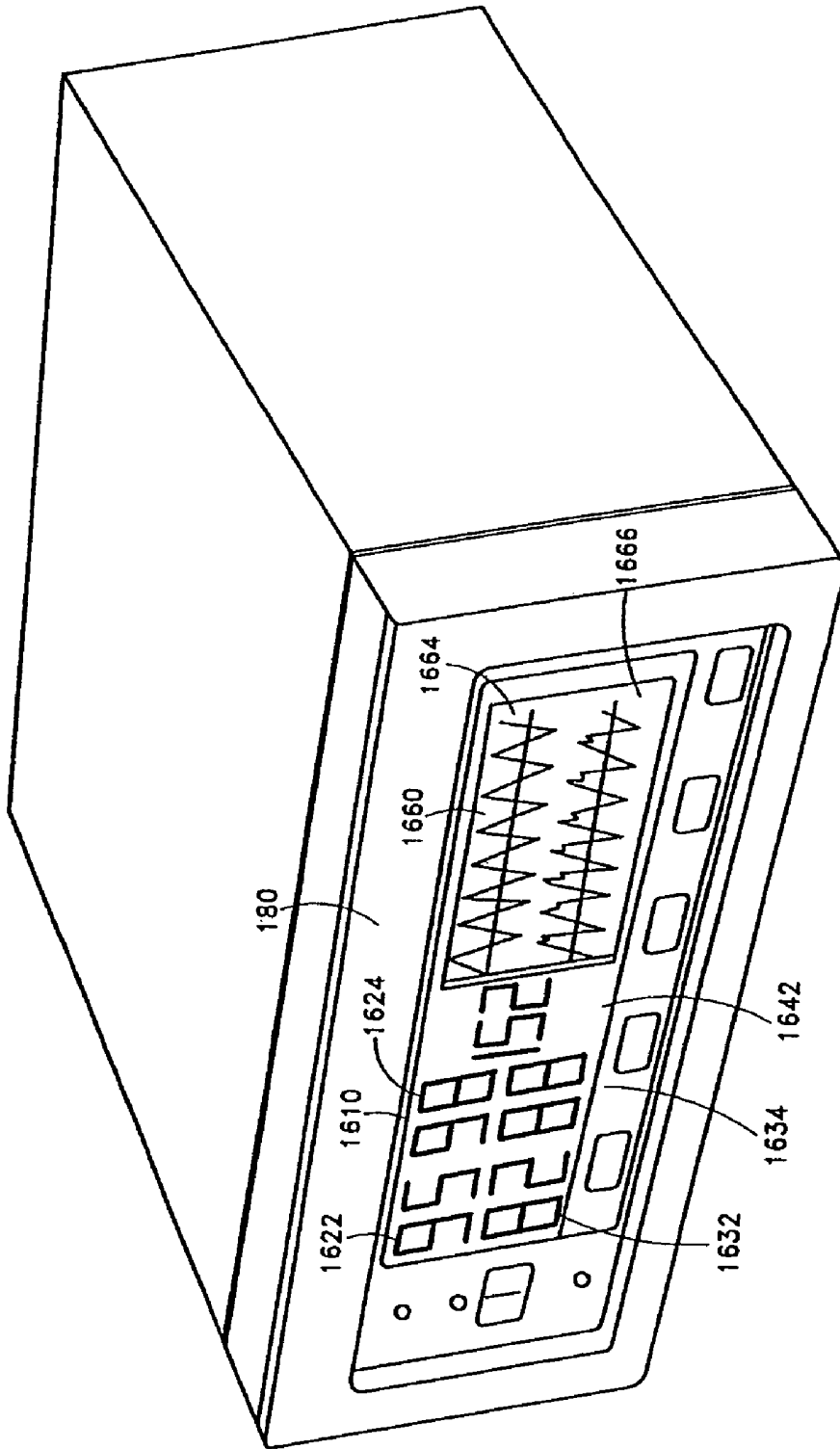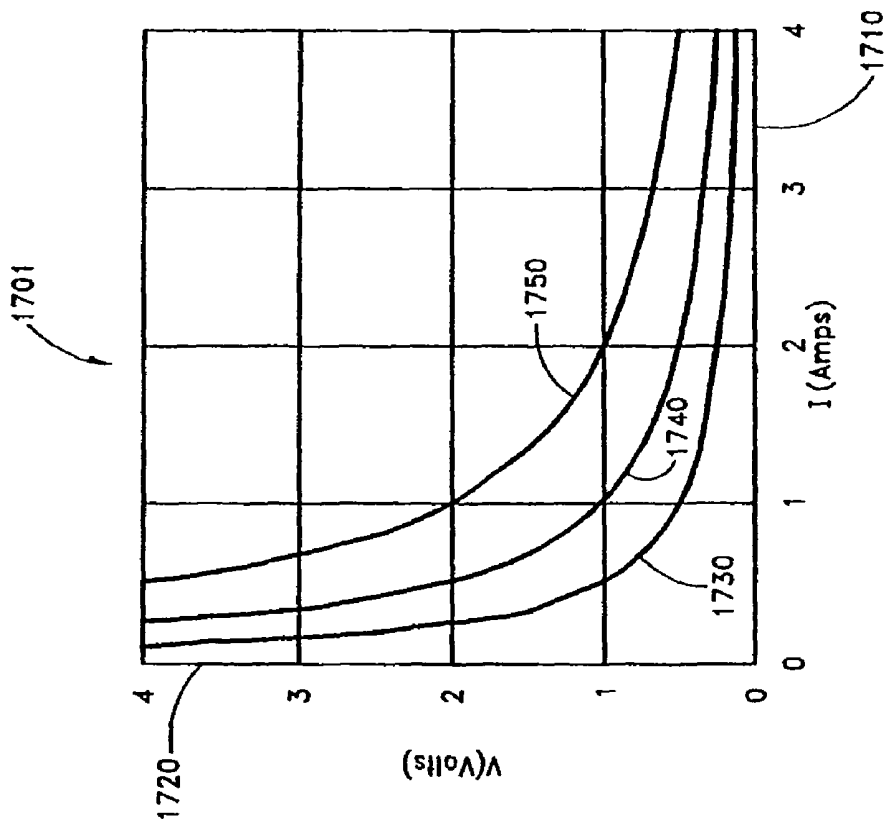
FIG. 8

FIG. 9

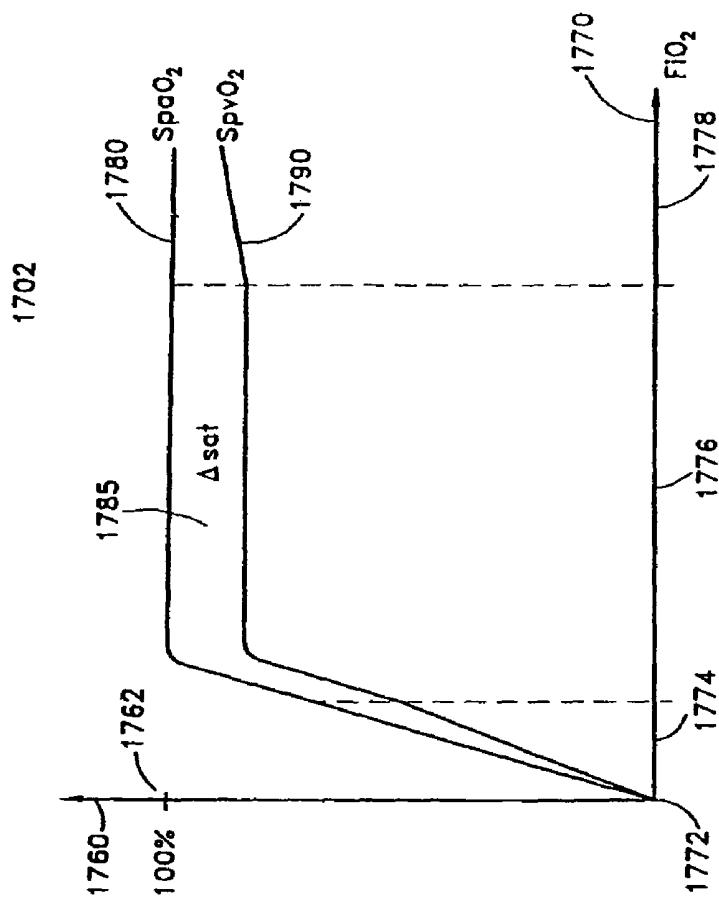*FIG. 10*

FIG. 11
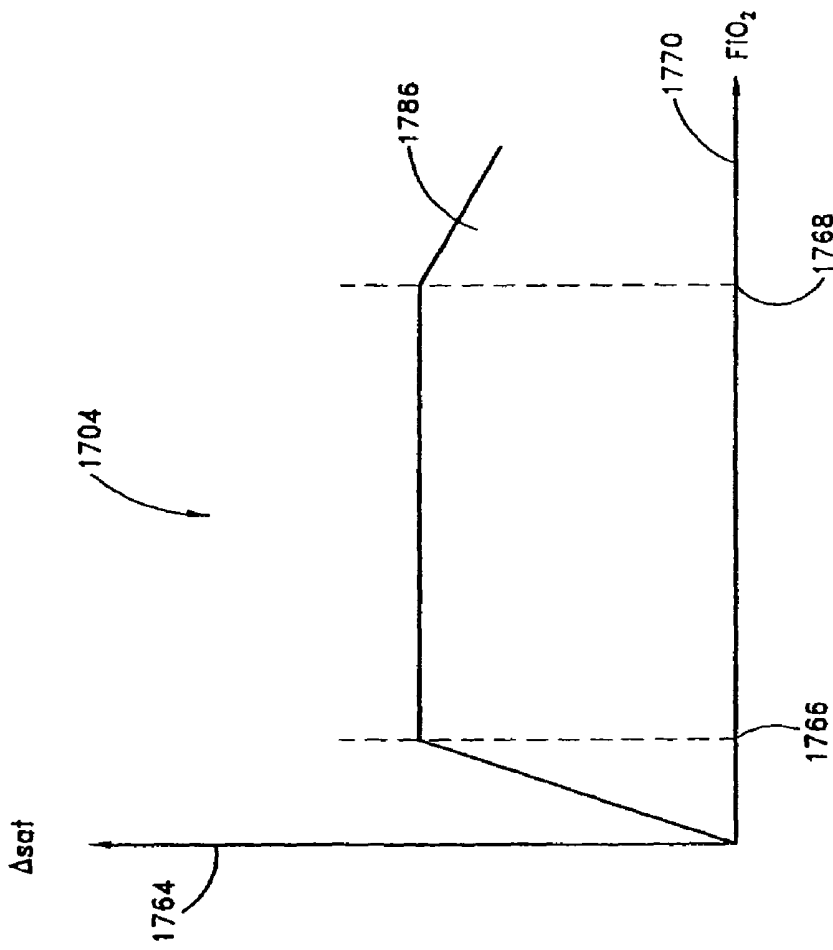
FIG. 12

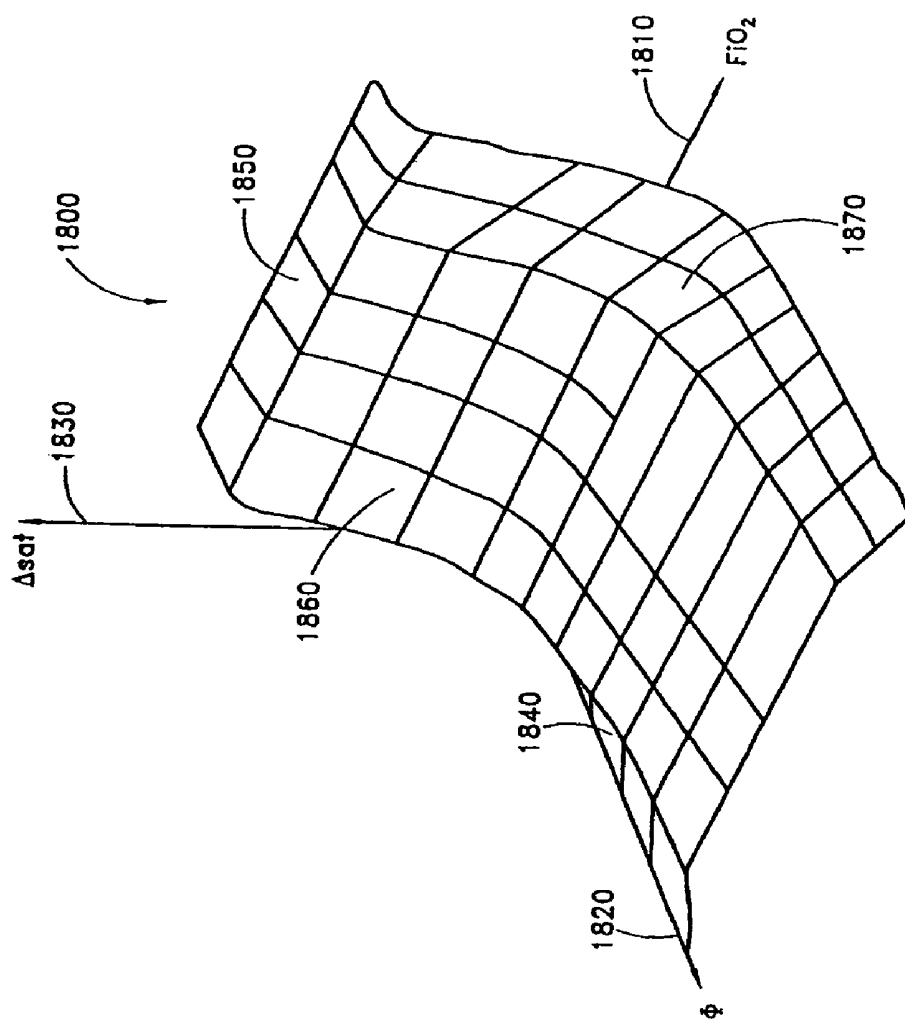FIG. 13

FIG. 14

FIG. 15

FIG. 16A

FIG. 16B
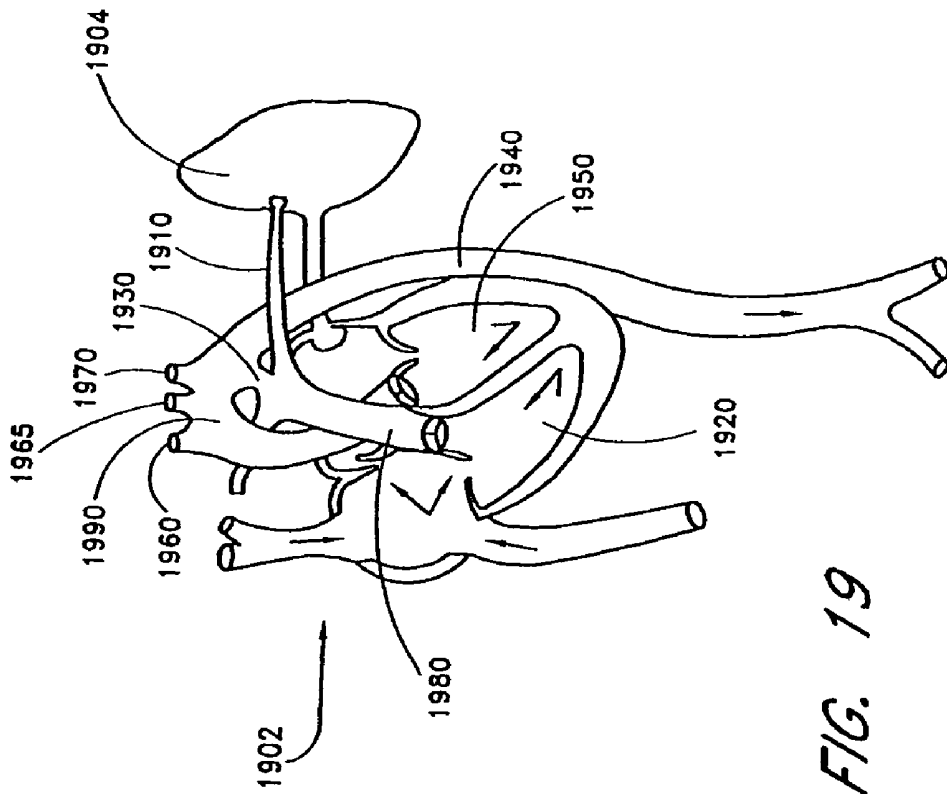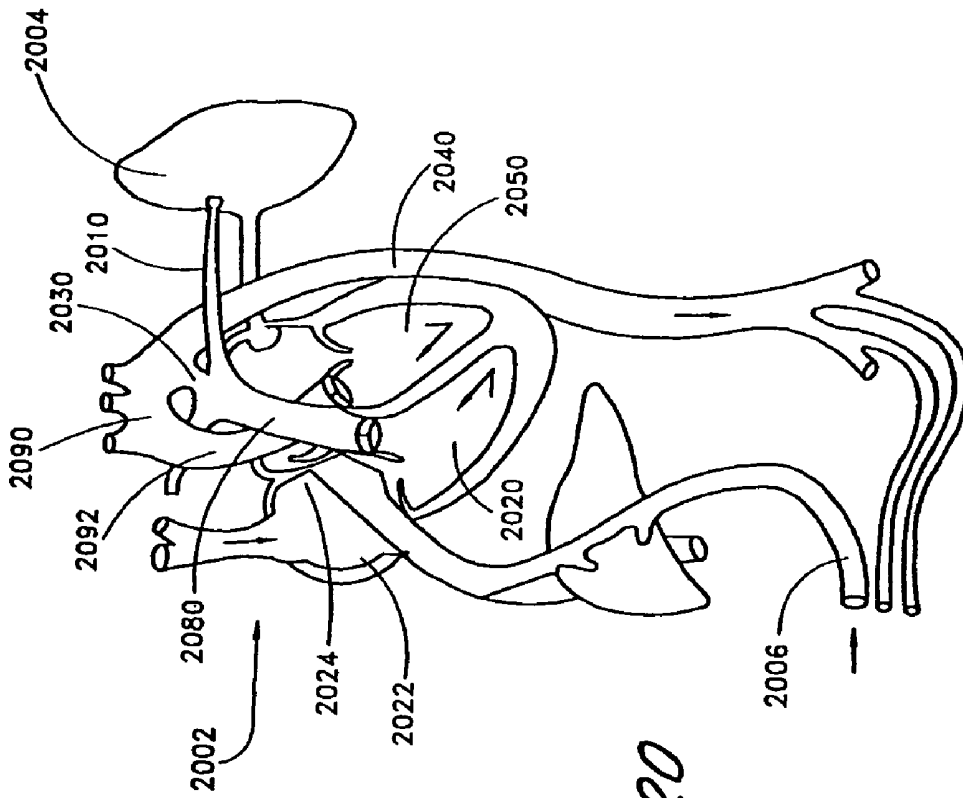
FIG. 17A

FIG. 17B

FIG. 17C
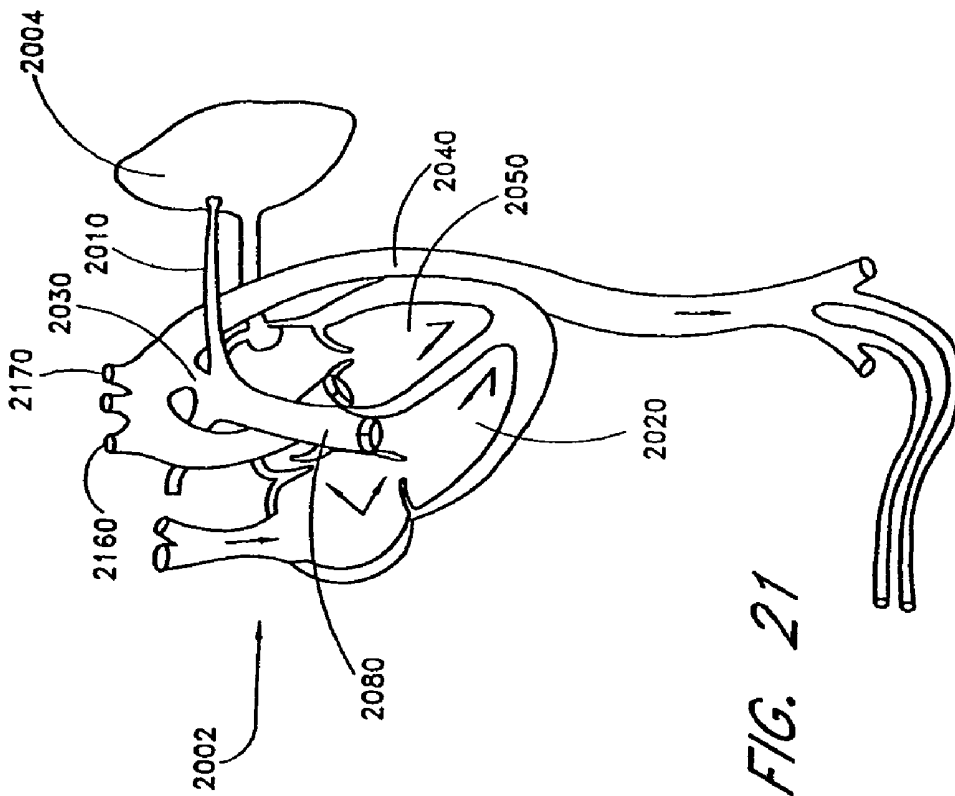
FIG. 18

FIG. 19

FIG. 20

FIG. 21

PHYSIOLOGICAL MONITOR

CROSS-REFERENCE TO RELATED APPLICATIONS

This application is a continuation of U.S. application Ser. No. 11/417,931, filed May 3, 2006, which is a continuation of U.S. application Ser. No. 11/104,720, filed Apr. 13, 2005, now U.S. Pat. No. 7,761,128, which is a continuation of U.S. application Ser. No. 10/668,487, filed Sep. 22, 2003, now U.S. Pat. No. 6,898,452, which is a continuation of U.S. application Ser. No. 10/026,013, filed Dec. 21, 2001, now U.S. Pat. No. 6,714,804, which is a continuation of U.S. application Ser. No. 09/323,176, filed May 27, 1999, now U.S. Pat. No. 6,334,065, which claims priority from U.S. Provisional No. 60/087,802, filed Jun. 3, 1998.

BACKGROUND

The measurement of oxygen delivery to the body and the corresponding oxygen consumption by its organs and tissues is vitally important to medical practitioners in the diagnosis and treatment of various medical conditions. Oxygen delivery, the transport of oxygen from the environment to organs and tissues, depends on the orchestration of several interrelated physiologic systems. Oxygen uptake is determined by the amount of oxygen entering the lung and the adequacy of gas exchange within the lung. This gas exchange is determined by the diffusion of oxygen from the alveolar space to the blood of the pulmonary capillaries. Oxygen is subsequently transported to all organs and tissues by blood circulation maintained by the action of the heart. The availability of oxygen to the organs and tissues is determined both by cardiac output and by the oxygen content in the blood. Oxygen content, in turn, is affected by the concentration of available hemoglobin and hemoglobin oxygen saturation. Oxygen consumption is related to oxygen delivery according to Fick's axiom, which states that oxygen consumption in the peripheral tissues is equal to oxygen delivery via the airway.

Oxygen delivery and oxygen consumption can be estimated from a number of measurable parameters. Because of the diagnostic impracticalities of measuring oxygen uptake and cardiac output, oxygen delivery is typically assessed from the oxygen status of arterial blood alone, such as arterial oxygen partial pressure, P_aO_2, and arterial oxygen saturation, S_aO_2. P_aO_2 represents the relatively small amount of oxygen dissolved in the blood plasma. S_aO_2 represents the much larger amount of oxygen chemically bound to the blood hemoglobin. Oxygen consumption is typically assessed from the oxygen status of mixed venous blood, i.e. the oxygen saturation of blood from the pulmonary artery, S_vO_2, which is used to estimate the O_2 concentration of blood returning from all tissues and organs of the body. These parameters can be measured by both invasive and non-invasive techniques, except S_vO_2, which requires an invasive measurement.

Invasive techniques include blood gas analysis using the in vitro measurement of extracted arterial or venous blood, drawn with a syringe and needle or an intervascular catheter. Arterial blood is commonly obtained by puncturing the brachial, radial or femoral artery. Venous blood can be obtained from an arm vein, but such a sample reflects only local conditions. To obtain mixed venous blood, which represents the composite of all venous blood, a long catheter is typically passed through the right heart and into the main pulmonary artery from a peripheral vein. Extracted blood gas analysis utilizes blood gas machines or oximeters. A blood gas machine measures the partial pressure of oxygen, PO_2, using

a "Clark electrode" that detects the current generated by oxygen diffusing to a sealed platinum electrode across a gas permeable membrane. An oximeter measures the oxygen saturation, SO_2, of oxygenated and deoxygenated hemoglobin using spectrophotometry techniques that detect the differential absorption of particular wavelengths of light by these blood components.

Invasive monitoring also includes the in vivo monitoring of blood gas via a catheter sensor inserted into an artery or vein. Miniaturization of the Clark electrode allows placement of the electrode in a catheter for continuous measurement of PO_2. A fiber optic equipped catheter attached to an external oximeter allows continuous measurement of oxygen saturation. Because of risks inherent in catheterization and the promotion of blood coagulation by certain sensors, these techniques are typically only used when vitally indicated.

Non-invasive techniques include pulse oximetry, which allows the continuous in vivo measurement of arterial oxygen saturation and pulse rate in conjunction with the generation of a photoplethysymograph waveform. Measurements rely on sensors which are typically placed on the fingertip of an adult or the foot of an infant. Non-invasive techniques also include transcutaneous monitoring of PO_2, accomplished with the placement of a heated Clark electrode against the skin surface. These non-invasive oxygen status measurement techniques are described in further detail below.

SUMMARY

Prior art invasive oxygen assessment techniques are inherently limited. Specifically, in vitro measurements, that is, blood extraction and subsequent analysis in a blood gas machine or an oximeter, are non-simultaneous and non-continuous. Further, in vivo measurements through catheterization are not casual procedures and are to be particularly avoided with respect to neonates. Prior art noninvasive techniques are also limited. In particular, conventional pulse oximeters are restricted to measurement of arterial oxygen saturation at a single patient site. Also, transcutaneous monitoring is similarly restricted to the measurement of an estimate of arterial partial pressure at a single patient site, among other limitations discussed further below.

The stereo pulse oximeter according to the present invention overcomes many of the limitations of prior art oxygen status measurements. The word "stereo" comes from the Greek word stereos, which means "solid" or three-dimensional. For example, stereophonic systems use two or more channels to more accurately reproduce sound. The stereo pulse oximeter is similarly multi-dimensional, providing simultaneous, continuous, multiple-site and multiple-parameter oxygen status and plethysmograph (photoplethysmograph) measurements. The stereo pulse oximeter provides a benefit in terms of cost and patient comfort and safety over invasive oxygen status estimation techniques. The multi-dimensional aspects of this invention further provide oxygen status and plethysmograph measurements not available from current noninvasive techniques. In addition, the stereo pulse oximeter allows the isolation of noise artifacts, providing more accurate oxygen status and plethysmograph measurements than available from conventional techniques. The result is improved patient outcome based on a more accurate patient assessment and better management of patient care.

In one aspect of the stereo pulse oximeter, data from a single sensor is processed to advantageously provide continuous and simultaneous multiple-parameter oxygen status and plethysmograph measurements from a particular tissue site. This is in contrast to a conventional pulse oximeter that pro-

vides only arterial oxygen saturation data from a tissue site. In particular a physiological monitor comprises a sensor interface and a signal processor. The sensor interface is in communication with a peripheral tissue site and has an output responsive to light transmitted through the site. The signal processor is in communication with the sensor interface output and provides a plurality of parameters corresponding to the oxygen status of the site, the plethysmograph features of the site or both. The parameters comprise a first value and a second value related to the peripheral tissue site. In one embodiment, the first value is an arterial oxygen saturation and the second value is a venous oxygen saturation. In this embodiment, another parameter provided may be the difference between arterial oxygen saturation and venous oxygen saturation at the tissue site. The venous oxygen saturation is derived from an active pulse generated at the site. The signal processor output may further comprise a scattering indicator corresponding to the site, and the sensor interface may further comprise a pulser drive, which is responsive to the scattering indicator to control the amplitude of the active pulse. One of the parameter values may also be an indication of perfusion.

In another aspect of the stereo pulse oximeter, data from multiple sensors is processed to advantageously provide continuous and simultaneous oxygen status measurements from several patient tissue sites. This is in contrast to a conventional pulse oximeter that processes data from a single sensor to provide oxygen status at a single tissue site. In particular, a physiological monitor comprises a plurality of sensor interfaces each in communications with one of a plurality of peripheral tissue sites. Each of the sensor interfaces has one of a plurality of outputs responsive to light transmitted through a corresponding one of the tissue sites. A signal processor is in communication with the sensor interface outputs and has a processor output comprising a plurality of parameters corresponding to the oxygen status of the sites, the plethysmograph features of the sites or both. The parameters may comprise a first value relating to a first of the peripheral tissue sites and a second value relating to a second of the peripheral tissue sites. In one embodiment, the first value and the second value are arterial oxygen saturations. In another embodiment, the first value and the second value are plethysmograph waveform phases. The physiological monitor may further comprise a sensor attachable to each of the tissue sites. This sensor comprises a plurality of emitters and a plurality of detectors, where at least one of the emitters and at least one of the detectors is associated with each of the tissue sites. The sensor also comprises a connector in communications with the sensor interfaces. A plurality of signal paths are attached between the emitters and the detectors at one end of the sensor and the connector at the other end of the sensor.

In yet another aspect of the stereo pulse oximeter, data from multiple sensors is processed to advantageously provide a continuous and simultaneous comparison of the oxygen status between several tissue sites. A conventional oximeter, limited to measurements at a single tissue site, cannot provide these cross-site comparisons. In particular a physiological monitoring method comprises the steps of deriving a reference parameter and a test parameter from oxygen status measured from at least one of a plurality of peripheral tissue sites and comparing that reference parameter to the test parameter so as to determine a patient condition. The reference parameter may be a first oxygen saturation value and the test parameter a second oxygen saturation value. In that case, the comparing step computes a delta oxygen saturation value equal to the arithmetic difference between the first oxygen saturation value and the second oxygen saturation value. In one embodiment, the reference parameter is an arterial oxygen saturation

measured at a particular one the tissue sites and the test parameter is a venous oxygen saturation measured at that particular site. In another embodiment, the reference parameter is a first arterial oxygen saturation value at a first of the tissue sites, the test parameter is a second arterial oxygen saturation value at a second of the tissue sites. In yet another embodiment, the reference parameter is a plethysmograph feature measured at a first of the sites, the test parameter is a plethysmograph feature measured at a second of the sites and the monitoring method comparison step determines the phase difference between plethysmographs at the first site and the second site. In a further embodiment, the comparing step determines a relative amount of damping between plethysmographs at the first site and the second site. The multi-dimensional features of these embodiments of the stereo pulse oximeter can be advantageously applied to the diagnosis and managed medical treatment of various medical conditions. Particularly advantageous applications of stereo pulse oximetry include oxygen titration during oxygen therapy, nitric oxide titration during therapy for persistent pulmonary hypertension in neonates (PPHN), detection of a patent ductus arteriosis (PDA), and detection of an aortic coarctation.

BRIEF DESCRIPTION OF THE DRAWINGS

The present invention will be described in detail below in connection with the following drawing figures in which:

FIG. 1A is a top-level block diagram of a stereo pulse oximeter according to the present invention;

FIG. 1B shows a single-sensor alternative embodiment to FIG. 1A;

FIG. 2 is a block diagram of the stereo pulse oximeter sensor interface;

FIG. 3 is a graph illustrating the absorption of red and infrared wavelengths by both oxygenated and deoxygenated hemoglobin;

FIG. 4 is a graph showing the empirical relationship between the "red over infrared" ratio and arterial oxygen saturation;

FIG. 5 is a block diagram of the analog signal conditioning for the sensor interface;

FIG. 6 is a functional block diagram of the stereo pulse oximeter signal processing;

FIG. 7 is a functional block diagram of the front-end signal processing;

FIG. 8 is a graph depicting the frequency spectrum of an arterial intensity signal;

FIG. 9 is a graph depicting the frequency spectrum of a combined arterial and venous intensity signal;

FIG. 10 is a functional block diagram of the saturation calculation signal processing;

FIG. 11 is a graph illustrating a plethysmograph waveform;

FIG. 12 is a graph illustrating the absorption contribution of various blood and tissue components;

FIG. 13 is a graph illustrating an intensity "plethysmograph" pulse oximetry waveform;

FIG. 14 is a functional block diagram of the plethysmograph feature extraction signal processing;

FIG. 15 is a functional block diagram of the multiple parameter signal processing;

FIG. 16A is an illustration of a single-site stereo pulse oximeter display screen;

FIG. 16B is an illustration of a multi-site stereo pulse oximeter display screen;

FIG. 17A is a graph depicting a family of constant power curves for the electrical analog of constant oxygen consumption;

FIG. 17B is a graph depicting arterial and venous oxygen saturation versus fractional inspired oxygen;

FIG. 17C is a graph depicting arterial minus venous oxygen saturation versus fractional inspired oxygen;

FIG. 18 is a three-dimensional graph depicting a delta oxygen saturation surface;

FIG. 19 is an illustration of a neonatal heart depicting a pulmonary hypertension condition;

FIG. 20 is an illustration of a fetal heart depicting the ductus arteriosis; and

FIG. 21 is an illustration of a neonatal heart depicting a patent ductus arteriosis (PDA).

DETAILED DESCRIPTION

Stereo Pulse Oximetry

FIG. 1A illustrates the multi-dimensional features of a stereo pulse oximeter 100 according to the present invention. Shown in FIG. 1A is an exemplary stereo pulse oximeter configuration in which a first sensor 110 is attached to a neonate's left hand, a second sensor 120 is attached to one of the neonate's feet, and a third sensor 130 is attached to the neonate's right hand. In general, these sensors are used to obtain oxygen status and photoplethysmograph measurements at peripheral sites, including a person's ears and face, such as the nose and regions of the mouth in addition to hands, feet and limbs, but not including internal sites such as internal organs and the brain.

Each sensor 110, 120, 130 provides a stream of data through a corresponding sensor interface 114, 124, 134 to the digital signal processor (DSP) 150. For example, the first sensor 110 is connected to an input 112 of the first sensor interface 114, and the output 118 of the first sensor interface 114 is attached to a first data channel input 152 of the DSP 150. Similarly, the second sensor 120 provides data to a second data channel input 154 and the third sensor 130 provides data to a third data channel input 158.

FIG. 1B illustrates an alternative embodiment of the separate sensors 110, 120, 130 (FIG. 1A). A stereo sensor 140 has multiple branches 112, 122, 132 each terminating in a sensor portion 114, 124, 134. Each sensor portion 114, 124, 134 has two light emitters and a light detector, as described below, and is attachable to a separate patient site. Thus, the stereo sensor 140 advantageously provides a single sensor device having multiple light emitters and multiple light detectors for attachment to multiple patient tissue sites. A combination of the stereo sensor 140 and a single patient cable 142 advantageously allows a single connection 144 at the stereo pulse oximeter 100 and a single connection 146 at the stereo sensor 140.

The DSP 150 can independently process each data channel input 152, 154, 158 and provide outputs 162 typical of pulse oximetry outputs, such as arterial oxygen saturation, Sp_aO_2, the associated plethysmograph waveform and the derived pulse rate. In contrast with a conventional pulse oximeter, however, these outputs 162 include simultaneous measurements at each of several patient tissue sites. That is, for the configuration of FIG. 1A, the stereo pulse oximeter 100 simultaneously displays Sp_aO_2 and an associated plethysmograph waveform for three tissue sites in addition to the patient's pulse rate obtained from any one of sites. Further, the DSP 150 can provide unique outputs unavailable from conventional pulse oximeters. These outputs 164 include venous oxygen saturation, Sp_vO_2, a comparison of arterial

and venous oxygen saturation, $\Delta_{sat} = Sp_{av}O_2 = Sp_aO_2 - Sp_vO_2$, and pleth, which denotes plethysmograph shape parameters, for each site. In addition, the DSP 150 can provide cross-site outputs that are only available using stereo pulse oximetry. These unique cross-site outputs 168 include $\Delta sat_{xy} = Sp_{ax}O_2 - Sp_{ay}O_2$, which denotes the arterial oxygen saturation at site x minus the arterial oxygen saturation at site y. Also included in these outputs 168 is $\Delta pleth_{xy}$, which denotes a comparison of plethysmograph shape parameters measured at site x and site y, as described in detail below. The stereo pulse oximeter also includes a display 180 capable of showing the practitioner the oxygen status and plethysmograph parameters described above. The display 180 has a multiple channel graphical and numerical display capability as described in more detail below.

Pulse Oximetry Sensor

FIG. 2 depicts one stereo pulse oximeter data channel having a sensor 110 and a sensor interface 114 providing a single data channel input 152 to the DSP 150. The sensor 110 is used to measure the intensity of red and infrared light after transmission through a portion of the body where blood flows close to the surface, such as a fingertip 202. The sensor 110 has two light emitters, each of which may be, for example, a light-emitting diode (LED). A red emitter 212, which transmits light centered at a red wavelength and an infrared (IR) emitter 214, which transmits light centered at an infrared wavelength are placed adjacent to, and illuminate, a tissue site. A detector 218, which may be a photodiode, is used to detect the intensity of the emitted light after it passes through, and is partially absorbed by, the tissue site. The emitters 212, 214 and detector 218 are secured to the tissue site, with emitters 212, 214 typically spaced on opposite sides of the tissue site from the detector 218.

To distinguish between tissue absorption at the two wavelengths, the red emitter 212 and infrared emitter 214 are modulated so that only one is emitting light at a given time. In one embodiment, the red emitter 212 is activated for a first quarter cycle and is off for the remaining three-quarters cycle; the infrared emitter 214 is activated for a third quarter cycle and is off for the remaining three-quarters cycle. That is, the emitters 212, 214 are cycled on and off alternately, in sequence, with each only active for a quarter cycle and with a quarter cycle separating the active times. The detector 218 produces an electrical signal corresponding to the red and infrared light energy attenuated from transmission through the patient tissue site 202. Because only a single detector 218 is used, it receives both the red and infrared signals to form a time-division-multiplexed (TDM) signal. This TDM signal is coupled to the input 112 of the sensor interface 114. One of ordinary skill in the art will appreciate alternative activation sequences for the red emitter 212 and infrared emitter 214 within the scope of this invention, each of which provides a time multiplexed signal from the detector 218 allowing separation of red and infrared signals and determination and removal of ambient light levels in downstream signal processing.

To compute Sp_aO_2, pulse oximetry relies on the differential light absorption of oxygenated hemoglobin, HbO_2, and deoxygenated hemoglobin, Hb, to compute their respective concentrations in the arterial blood. This differential absorption is measured at the red and infrared wavelengths of the sensor 110. The relationship between arterial oxygen saturation and hemoglobin concentration can be expressed as:

$$Sp_aO_2 = 100\frac{C_{HbO2}}{C_{Hb} + C_{HbO2}} \quad (1)$$

That is, arterial oxygen saturation is the percentage concentration of oxygenated hemoglobin compared to the total concentration of oxygenated hemoglobin and deoxygenated hemoglobin in the arterial blood. Sp_aO_2 is actually a measure of the partial oxygen saturation of the hemoglobin because other hemoglobin derivatives, such as COHb and MetHb, are not taken into consideration.

FIG. **3** shows a graph **300** of the optical absorption properties of HbO_2 and Hb. The graph **300** has an x-axis **310** corresponding to wavelength and a y-axis **320** corresponding to hemoglobin absorption. An Hb curve **330** shows the light absorption properties of deoxygenated hemoglobin. An HbO_2 curve **340** shows the light absorption properties of oxygenated hemoglobin. Pulse oximetry measurements are advantageously made at a red wavelength **350** corresponding to 660 nm and an infrared wavelength **360** corresponding to 905 nm. This graph **300** shows that, at these wavelengths **350**, **360**, deoxygenated hemoglobin absorbs more red light than oxygenated hemoglobin, and, conversely, oxygenated hemoglobin absorbs more infrared light than deoxygenated hemoglobin.

In addition to the differential absorption of hemoglobin derivatives, pulse oximetry relies on the pulsatile nature of arterial blood to differentiate hemoglobin absorption from absorption of other constituents in the surrounding tissues. Light absorption between systole and diastole varies due to the blood volume change from the inflow and outflow of arterial blood at a peripheral tissue site. This tissue site might also comprise skin, muscle, bone, venous blood, fat, pigment, etc., each of which absorbs light. It is assumed that the background absorption due to these surrounding tissues is invariant and can be ignored. Thus, blood oxygen saturation measurements are based upon a ratio of the time-varying or AC portion of the detected red and infrared signals with respect to the time-invariant or DC portion. This AC/DC ratio normalizes the signals and accounts for variations in light pathlengths through the measured tissue. Further, a ratio of the normalized absorption at the red wavelength over the normalized absorption at the infrared wavelength is computed:

$$\frac{RD}{IR} = \frac{\left(\frac{Red_{AC}}{Red_{DC}}\right)}{\left(\frac{IR_{AC}}{IR_{DC}}\right)} \quad (2)$$

where Red_{AC}, and IR_{AC} are the root-mean-square (RMS) of the corresponding time-varying signals. This "red-over-infrared, ratio-of-ratios" cancels the pulsatile signal. The desired Sp_aO_2 measurement is then computed from this ratio.

FIG. **4** shows a graph **400** depicting the relationship between RD/IR and Sp_aO_2. This relationship can be approximated from Beer-Lambert's Law, as outlined below. However, it is most accurately determined by statistical regression of experimental measurements obtained from human volunteers and calibrated measurements of oxygen saturation. The result can be depicted as a curve **410**, with measured values of RD/IR shown on a y-axis **420** and corresponding saturation values shown on an x-axis **430**. In a pulse oximeter device, this empirical relationship can be stored in a read-only memory (ROM) look-up table so that Sp_aO_2 can be directly read-out from input RD/IR measurements.

According to the Beer-Lambert law of absorption, the intensity of light transmitted through an absorbing medium is given by:

$$I = I_0 \exp\left(-\sum_{i=1}^{N} \varepsilon_{i\lambda} c_i x_i\right) \quad (3)$$

where I_0 is the intensity of the incident light, $\epsilon_{i,\lambda}$ is the absorption coefficient of the ith constituent at a particular wavelength λ, c_i is the concentration coefficient of the ith constituent and x_i is the optical path length of the ith constituent. As stated above, assuming the absorption contribution by all constituents but the arterial blood is constant, taking the natural logarithm of both sides of equation (3) and removing time invariant terms yields:

$$In(I) = -[\epsilon_{HbO2,\lambda}C_{HbO2} + \epsilon_{Hb,\lambda}C_{hb}]x(t) \quad (4)$$

Measurements taken at both red and infrared wavelengths yield:

$$RD(t) = -[\epsilon_{HbO2,RD}C_{HbO2} + \epsilon_{Hb,RD}C_{hb}]x_{RD}(t) \quad (5)$$

$$IR(t) = -[\epsilon_{HbO2,IR}C_{HbO2} + \epsilon_{Hb,IR}C_{hb}]x_{IR}(t) \quad (6)$$

Taking the ratio RD(t)/IR(t) and assuming $x_{RD}(t) \approx x_{IR}(t)$ yields:

$$RD/IR = [\epsilon_{HbO2,RD}C_{HbO2} + \epsilon_{Hb,RD}C_{Hb}]/[\epsilon_{HbO2,IR}C_{HbO2} + \epsilon_{Hb,IR}C_{hb}] \quad (7)$$

Assuming further that:

$$C_{HbO2} + C_{Hb} = 1 \quad (8)$$

then equation (1) can be solved in terms of RD/IR yielding a curve similar to the graph **400** of FIG. **4**.

Sensor Interface

FIG. **2** also depicts the sensor interface **114** for one data channel. An interface input **112** from the sensor **110** is coupled to an analog signal conditioner **220**. The analog signal conditioner **220** has an output **223** coupled to an analog-to-digital converter (ADC) **230**. The ADC output **118** is coupled to the DSP **150**. The analog signal conditioner also has a gain control input **225** from the DSP **150**. The functions of the analog signal conditioner **220** are explained in detail below. The ADC **230** functions to digitize the input signal **112** prior to further processing by the DSP **150**, as described below. The sensor interface **114** also has an emitter current control input **241** coupled to a digital-to-analog converter (DAC) **240**. The DSP provides control information to the DAC **240** via the control input **241** for a pair of emitter current drivers **250**. One driver output **252** couples to the red emitter **212** of the sensor **110**, and another driver output **254** couples to the IR emitter **214** of the sensor **110**.

FIG. **5** illustrates one embodiment of the analog signal conditioner **220**. The analog signal conditioner **220** receives a composite intensity signal **112** from the sensor detector **218** (FIG. **2**) and then filters and conditions this signal prior to digitization. The embodiment shown has a preamplifier **510**, a high pass filter **520**, a programmable gain amplifier **530** and a low pass filter **540**. The low pass filter output **223** is coupled to the ADC **230** (FIG. **2**). The preamplifier **510** converts the current signal **112** from the detector **218** (FIG. **2**) to a corresponding amplified voltage signal. The gain in the preamplifier **510** is selected in order to prevent ambient light in the signal **112** from saturating the preamplifier **510** under normal operating conditions. The preamplifier output **512** is coupled to the high pass filter **520**, which removes the DC component of the detector signal **112**. The corner frequency of the high

pass filter **520** is set well below the multiplexing frequency of the red and infrared emitters **212, 214** (FIG. **2**). The high pass filter output **522** couples to the programmable gain amplifier **530**, which also accepts a programming input **225** from the DSP **150** (FIG. **2**). This gain is set at initialization or at sensor placement to compensate for variations from patient to patient. The programmable gain amplifier output **532** couples to a low-pass filter **540** to provide anti-aliasing prior to digitization.

As described above, pulse oximetry measurements rely on the existence of a pulsatile signal. The natural heart beat provides a pulsatile signal that allows measurement of arterial oxygen saturation. In the systemic circulation, all arterial pulsations are damped before flow enters the capillaries, and none are transmitted into the veins. Thus, there is no arterial pulse component in the venous blood and absorption caused by venous blood is assumed canceled by the ratio-of-ratio operation described above. Venous blood, being at a relatively low pressure, will "slosh back and forth" during routine patient motions, such as shivering, waving and tapping. This venous blood sloshing creates a time-varying signal that is considered "noise" and can easily overwhelm conventional ratio-based pulse oximeters. Advanced pulse oximetry techniques allow measurement of Sp_vO_2 under these circumstances. For example, such advanced techniques are disclosed in U.S. Pat. No. 5,632,272, which is assigned to the assignee of the current application. This measurement is only available during motion or other physiological events causing a time-varying venous signal.

The venous blood may also have a pulsatile component at the respiration rate, which can be naturally induced or ventilator induced. In adults, the natural respiration rate is 10-15 beats per minute (bpm). In neonates, this natural respiration rate is 30-60 bpm. The ventilator induced pulse rate depends on the ventilator frequency. If this respiration induced venous pulse is of sufficient magnitude, advanced pulse oximetry techniques, described below, allow measurement of Sp_vO_2.

A controlled physiological event, however, can be created that allows for a continuous measurement of venous oxygen saturation, independent of motion or respiration. U.S. Pat. No. 5,638,816, which is assigned to the assignee of the current application discloses a technique for inducing an intentional active perturbation of the blood volume of a patient, and is referred to as an "active pulse." Because peripheral venous oxygen saturation, Sp_vO_2, is a desirable parameter for stereo pulse oximetry applications, it is advantageous to provide for a continuous and controlled pulsatile venous signal.

FIG. **2** depicts an active pulse mechanism used in conjunction with a pulse oximetry sensor. An active pulser **260** physically squeezes or otherwise perturbs a portion of patient tissue **270** in order to periodically induce a "pulse" in the blood at the tissue site **202**. A pulser drive **280** generates a periodic electrical signal to a transducer **262** attached to the patient. The transducer **262** creates a mechanical force against the patient tissue **270**. For example, the pulser **260** could be a solenoid type device with a plunger that presses against the fleshy tissue to which it is attached. The DSP **150** provides pulse drive control information to a digital to analog converter (DAC) **290** via the control input **291**. The DAC output **292** is coupled to the pulser drive **280**. This allows the processor to advantageously control the magnitude of the induced pulse, which moderates scattering as described below. The pulser **260** could be a pressure device as described above. Other pressure mechanisms, for example a pressure cuff, could be similarly utilized. Other methods, such as temperature fluctuations or other physiological changes, which physiologically alter a fleshy medium of the body on a periodic basis to

modulate blood volume at a nearby tissue site could also be used. Regardless of the active pulse mechanism, this modulated blood volume is radiated by a pulse oximeter sensor and the resulting signal is processed by the signal processing apparatus described below to yield Sp_vO_2.

Signal Processor

FIG. **6** illustrates the processing functions of the digital signal processor (DSP) **150** (FIG. **1A**). Each data channel input **152, 154, 158** (FIG. **1A**) is operated on by one or more of the front-end processor **610**, saturation calculator **620**, plethysmograph feature extractor **630** and multiple parameter processor **640** functions of the DSP **150**. First, a digitized signal output from the ADC **230** (FIG. **2**) is input **602** to the front-end processor **610**, which demultiplexes, filters, normalizes and frequency transforms the signal, as described further below. A front-end output **612** provides a red signal spectrum and an IR signal spectrum for each data channel as inputs to the saturation calculator **620**. Another front-end output **614** provides a demultiplexed, normalized IR plethysmograph for each data channel as an input to the feature extractor **630**. The saturation calculator output **622** provides arterial and venous saturation data for each data channel as input to the multiple parameter processor **640**. One feature extractor output **632** provides data on various plethysmograph shape parameters for each data channel as input into the multiple parameter processor **640**. Another feature extractor output **634**, also coupled to multiple parameter processor **640**, provides an indication of plethysmograph quality and acts as a threshold for determining whether to ignore portions of the input signal **602**. The multiple parameter processor has a numerical output **642** that provides same-channel Δsat parameters and cross-channel parameters, such as Δsat_{xy} or $\Delta pleth_{xy}$ to a display **180** (FIG. **1A**). The numeric output **642** may also provide saturation and plethysmograph parameters directly from the saturation calculator **620** or the feature extractor **630** without further processing other than data buffering. The multiple parameter processor also has a graphical output **644** that provides plethysmograph waveforms for each data channel in addition to graphics, depending on a particular application, the indicate the trend of the numerical parameters described above.

Front-End Processor

FIG. **7** is a functional block diagram of the front-end processor **610** for the stereo pulse oximeter. The digitized sensor output **118** (FIG. **2**) is an input signal **602** to a demultiplexer **710**, which separates the input signal **602** into a red signal **712** and an infrared signal **714**. The separated red and infrared signals **712, 714** are each input to a filter **720** to remove unwanted artifacts introduced by the demultiplexing operation. In one embodiment, the filter **720** is a finite-impulse-response, low-pass filter that also "decimates" or reduces the sample rate of the red and infrared signals **712, 714**. The filtered signals **722** are then each normalized by a series combination of a log function **730** and bandpass filter **740**. The normalized signals, RD(t), IR(t) **742** are coupled to a Fourier transform **750**, which provides red frequency spectrum and infrared frequency spectrum outputs, RD(ω), IR(ω) **612**. A demultiplexed infrared signal output **614** is also provided.

Saturation Calculator

FIG. **8** shows a graph **800** illustrating idealized spectrums of RD(t) and IR(t) **752** (FIG. **7**). The graph has an x-axis **810** that corresponds to the frequency of spectral components in these signals and a y-axis **820** that corresponds to the magnitude of the spectral components. The spectral components are the frequency content of RD(t) and IR(t), which are plethysmograph signals corresponding to the patient's pulsatile

blood flow, as described below. Thus, the frequencies shown along the x-axis **810**, i.e. f_0, f_1, f_2, are the fundamental and harmonics of the patient's pulse rate. The spectrum of RD(t), denoted RD(ω) **612** (FIG. **7**), is shown as a series of peaks, comprising a first peak **832** at a fundamental frequency, f_0, a second peak **842** at a first harmonic, f_1 and a third peak **852** at a second harmonic, f_2. Similarly, the spectrum of IR(t), denoted IR(ω) **612** (FIG. **7**), is shown as another series of peaks, comprising a first peak **834** at a fundamental frequency, f_0, a second peak **844** at a first harmonic, f_1 and a third peak **854** at a second harmonic, f_2. Also shown in FIG. **8** is the ratio of the spectral peaks of RD(t) and IR(t), denoted RD(ω)/IR(ω). This ratio is shown as a first ratio line **838** at the fundamental frequency f_0, a second ratio line **848** at the first harmonic f_1, and a third ratio line **858** at the second harmonic f_2.

The magnitude of these ratio lines RD(ω)/IR(ω) corresponds to the ratio RD/IR defined by equation (2), and, hence, can be used to determine Sp_aO_2. This can be seen from Parseval's relation for a periodic signal, x(t), having a period T, where X_k is the spectral component at the kth harmonic of x(t):

$$\frac{1}{T}\int_0^T (|x(t)|)^2\,dt = \sum_k (|X_k|)^2 \qquad (9)$$

Equation (9) relates the energy in one period of the signal x(t) to the sum of the squared magnitudes of the spectral components. The term $|X_k|^2$ can be interpreted as that part of the energy per period contributed by the kth harmonic. In an ideal measurement, the red and infrared signals are the same to within a constant scale factor, which corresponds to the arterial oxygen saturation. Likewise, the red and infrared spectra are also the same to within a constant scale factor. Thus, in an ideal measurement, all of the ratio lines **838**, **848**, **858** have substantially the same amplitude. Any differences in the amplitude of the ratio lines is likely due to motion, scattering or other noise contaminations, as discussed further below. Accordingly, any of the RD(ω)/IR(ω) ratio lines is equivalent to the ratio, RD/IR, of equation (2) and can be used to derive Sp_aO_2.

One skilled in the art will recognize that the representations in FIG. **8** are idealized. In particular, in actual measured data, especially if contaminated by noise, the frequencies of the peaks of RD(ω) do not correspond exactly to the frequencies of the peaks of IR(ω). For example, the fundamental frequency, f_0, found for RD(ω) will often be different from the fundamental frequency, f_0', found for IR(ω) and similarly for the harmonics of f_0.

FIG. **9** shows a graph **900** illustrating idealized spectrums RD(ω) and IR(ω) and associated ratio lines measured with an active pulse sensor. The graph **900** has an x-axis **910** that corresponds to the frequency of spectral components in these signals and a y-axis **920** that corresponds to the magnitude of the spectral components. The spectrum, RD(ω), is shown as two series of peaks. One series of peaks **930** occurs at a fundamental frequency, f_{h0}, and associated harmonics, f_{h1} and f_{h2}, of the patient's pulse (heart) rate. Another series of peaks **940** occurs at a fundamental frequency, f_{p0}, and associated harmonics, f_{p1} and f_{p2}, of the active pulse rate. Similarly, the spectrum, IR(ω), is shown as two series of peaks. One series of peaks **950** occurs at a fundamental frequency, f_{h0}, and associated harmonics, f_{h1} and f_{h2}, of the patient's pulse rate. Another series of peaks **960** occurs at a fundamental frequency, f_{p0}, and associated harmonics, f_{p1} and f_{p2}, of the

active pulse rate. Accordingly, there are two series of RD/IR ratio lines. One series of ratio lines **970** are at the patient's pulse rate and associated harmonics, and another series of ratio lines **980** are at the active pulser rate and associated harmonics.

Because only the arterial blood is pulsatile at the patient's pulse rate, the ratio lines **970** are only a function of the arterial oxygen saturation. Accordingly, Sp_aO_2 can be derived from the magnitude of these ratio lines **970**, as described above. Further, a modulation level for the active pulse is selected which insignificantly perturbates the arterial blood while providing a measurable venous signal. This is possible because the arterial blood pressure is significantly larger than the venous pressure. The modulation level is regulated as described above with respect to FIG. **2**, i.e. the DSP **150**, via a pulser drive control **291**, sets the magnitude of the pulser drive **280** to the pulse inducing mechanism **262**. Assuming that the active pulse modulation of the arterial blood is insignificant, only the venous blood is pulsatile at the active pulser rate. Hence, the ratio lines **980** are only a function of the venous oxygen saturation. Accordingly, Sp_aO_2 can be derived from the magnitude of the pulse rate related ratio lines **980** in the same manner as Sp_aO_2 is derived from the magnitude of the pulse rate related ratio lines.

Scattering

Propagation of optical radiation through tissue is affected by absorption and scattering processes. The operation of pulse oximeters was described qualitatively above using an analysis based on the Beer-Lambert law of absorption, equation (3). This approach, however, fails to account for the secondary effects of light scattering at pulse oximeter wavelengths. The primary light scatterer in blood is erythrocytes, i.e. red blood cells. A qualitative understanding of the effects of scattering on pulse oximetry is aided by a description of red blood cell properties within flowing blood.

Human blood is a suspension of cells in an aqueous solution. The cellular contents are essentially all red blood cells, with white cells making up less the $\frac{1}{600}^{th}$ of the total cellular volume and platelets less than $\frac{1}{800}^{th}$ of the total cellular volume. Normally the hematocrit, which is the percentage of the total volume of blood occupied by cells, is about 50% in large vessels and 25% in small arterioles or venules.

Red blood cells are extremely deformable, taking on various shapes in response to the hydrodynamic stresses created by flowing blood. For example, assuming a laminar blood flow within a vessel, a parabolic velocity profile exists that is greatest in the vessel center and smallest along the vessel walls. Nominally, red blood cells are shaped as biconcave disks with a diameter of 7.6 um and thickness of 2.8 um. Exposed to this velocity profile, the red blood cells become parachute-shaped and aligned in the direction of the blood flow. Thus, during systole, transmitted light is scattered by aligned, parachute-shaped cells. During diastole, the light is scattered by biconcave disks having a more or less random alignment.

The time-varying shape and alignment of the red blood cells can have a significant effect on measured values of oxygen saturation if scattering is ignored. Analogous to the analysis using the Beer-Lambert absorption law, scattering can be qualitatively understood as a function of the scattering coefficients of various tissues. Specifically, the bulk scattering coefficient can be written as:

$$\mu_s = V_b\mu_b + V_t\mu_t \qquad (10)$$

where V_b is the blood volume, $-\mu_b$ is the scattering coefficient of blood, V_t is the surrounding tissue volume and $-\mu_t$ is the scattering coefficient of the surrounding tissue. The volume,

V_t, and scattering coefficient, $-\mu_t$, of the surrounding tissue are time invariant. The blood volume, V_b, however, is pulsatile. The ratio of ratios computation, RD/IR, results in normalization of the time invariant or DC tissue absorption and cancellation of the time varying or AC pulsatile blood volume absorption to yield a number related to oxygen saturation. This computational approach is valid because the absorption coefficients of blood, $\epsilon_{HbO2,\lambda}$, $\epsilon_{Hb,\lambda}$ given in equation (4) were assumed to change only slowly over time. The scattering coefficient of blood $-\mu_b$, however, is time variant. As described above, this variation is due to the time-varying alignment and shape of the red blood cells. This time variation in the detected intensity of light transmitted through a tissue site is not normalized or canceled by the RD/IR calculation. Further, because the magnitude of the scattering coefficient variations is a function of blood flow, these variations become more pronounced with larger pulses in the blood supply. As a result, scattering produces frequency-dependent magnitude variations in the ratio lines $RD(\omega)/IR(\omega)$.

FIG. 9 illustrates the effect of scattering on the spectra of the detected red and infrared intensity waveforms. When these waveforms are transformed into the frequency domain, the time varying component of scattering manifests itself as spreads 978, 988 in the RD/IR ratio lines at each harmonic of the plethysmograph or active pulse rate. The magnitude of the ratio lines 970 at the fundamental and harmonics of the patient's pulse rate varies between a minimum 972 and a maximum 974, resulting in a magnitude spread 978. Similarly, the magnitude of the ratio lines 980 at the fundamental and harmonics of the active pulse rate varies between a minimum 982 and a maximum 984, resulting in a magnitude spread 988. Normally, absent motion artifact or noise contamination, the spread 978, 988 in the ratio lines is quiet small, but the magnitude of these spreads 978, 988, increases with larger blood flows or pulse magnitudes. Scattering attributable to an active pulse can be regulated by adjusting the magnitude of the active pulse modulation based upon the amount of spread 978, 988 of the ratio line magnitudes. Thus, the active pulse magnitude can be increased to obtain a larger detected AC signal, but limited to below the point at which scattering becomes significant.

FIG. 10 depicts an embodiment of the signal processing for determining oxygen saturation from the ratio lines of $RD(\omega)/RD(\omega)$. The red spectrum $RD(\omega)$ 612 and infrared spectrum $IR(\omega)$ 612, computed as described above with respect to FIG. 7, are input to a peak detector 1010. The peak detector 1010 separately calculates localized maximums for $RD(\omega)$ and $IR(\omega)$. The peak detector output 1012 is a series of frequencies corresponding to the patient pulse rate fundamental and harmonics. If an active pulse is used, the peak detector output 1012 is also a series of frequencies corresponding to the active pulse rate. Although the active pulse rate is known, the detected peaks may have been shifted due to noise, motion artifact or other signal contamination. The peak detector output 1012 is coupled to a series combination of peak matcher 1020 and ratio line calculator 1030. The ratio lines RD/IR are calculated by matching the frequency peaks of $RD(\omega)$ with the nearest frequency peaks of $IR(\omega)$. The ratio lines associated with the pulse rate harmonics 1032 are then separated into a different set from the ratio lines associated with the active pulse harmonics 1034, assuming an active pulse is utilized. An average ratio line for each set 1032, 1034 is calculated by averaging 1060 all ratio lines in a set. The magnitude of the average ratio line r 1062 for the pulse rate set 1032 is then fed to a look-up table (LUT) 1090, which provides an output 622 of the measured value of Sp_aO_2. Similarly, if an active pulse is used, the magnitude of the average

ratio line μ 1064 for the active pulse rate set 1034 is then fed to a LUT 1090, which provides an output 622 of the measured value of Sp_vO_2. A scattering detector 1080 computes the spread 988 (FIG. 9) in the set of ratio lines associated with the active pulse and provides this value 1082 to the DSP 150 (FIG. 2) so that the DSP can set the pulser drive control 291 (FIG. 2) to regulate the magnitude of the active pulse.

Alternatively, Sp_vO_2 may be measured from respiration-induced pulses in the venous blood, described above, without utilizing an active pulse sensor. Specifically, a series of ratio lines 980 (FIG. 9) would occur at a fundamental frequency, f_{r0}, and associated harmonics, f_{r1} and f_{r2}, of the respiration rate, which is either known from the ventilator frequency or derived from a separate measurement of the natural respiration. As shown in FIG. 10, the ratio lines associated with the respiration rate harmonics 1034 are then separated into a different set from the ratio lines associated with the pulse rate harmonics 1032. An average ratio line for the respiration rate set 1034 is calculated by averaging 1060 all ratio lines in that set. The magnitude of the average ratio line μ 1064 for the respiration rate set 1034 is then fed to a look-up table (LUT) 1090, which provides an output 622 of the measured value of Sp_vO_2.

Plethysmograph Feature Extractor

FIG. 11 illustrates the standard plethysmograph waveform 1100, which can be derived from a pulse oximeter. The waveform 1100 is a visualization of blood volume change in the illuminated peripheral tissue caused by arterial blood flow, shown along the y-axis 1110, over time, shown along the x-axis 1120. The shape of the plethysmograph waveform 1100 is a function of heart stroke volume, pressure gradient, arterial elasticity and peripheral resistance. The ideal waveform 1100 displays a broad peripheral flow curve, with a short, steep inflow phase 1130 followed by a 3 to 4 times longer outflow phase 1140. The inflow phase 1130 is the result of tissue distention by the rapid blood volume inflow during ventricular systole. During the outflow phase 1140, blood flow continues into the vascular bed during diastole. The end diastolic baseline 1150 indicates the minimum basal tissue perfusion. During the outflow phase 1140 is a dicrotic notch 1160, the nature of which is disputed. Classically, the dicrotic notch 1160 is attributed to closure of the aortic valve at the end of ventricular systole. However, it may also be the result of reflection from the periphery of an initial, fast propagating, pressure pulse that occurs upon the opening of the aortic valve and that precedes the arterial flow wave. A double dicrotic notch can sometimes be observed, although its explanation is obscure, possibly the result of reflections reaching the sensor at different times.

FIG. 12 is a graph 1200 illustrating the absorption of light at a tissue site illuminated by a pulse oximetry sensor. The graph 1200 has a y-axis 1210 representing the total amount of light absorbed the tissue site, with time shown along an x-axis 1220. The total absorption is represented by layers including the static absorption layers due to tissue 1230, venous blood 1240 and a baseline of arterial blood 1250. Also shown is a variable absorption layer due to the pulse-added volume of arterial blood 1260. The profile 1270 of the pulse-added arterial blood 1260 is seen as the plethysmograph waveform 1100 depicted in FIG. 11.

FIG. 13 illustrates the photoplethysmograph intensity signal 1300 detected by a pulse oximeter sensor. A pulse oximeter does not directly detect absorption, and hence does not directly measure the standard plethysmograph waveform 1100 (FIG. 11). However, the standard plethysmograph can be derived by observing that the detected intensity signal 1300 is merely an out of phase version of the absorption

15   16

profile **1270**. That is, the peak detected intensity **1372** occurs at minimum absorption **1272** (FIG. **12**), and minimum detected intensity **1374** occurs at maximum absorption **1274** (FIG. **12**). Further, a rapid rise in absorption **1276** (FIG. **12**) during the inflow phase of the plethysmograph is reflected in a rapid decline **1376** in intensity, and the gradual decline **1278** (FIG. **12**) in absorption during the outflow phase of the plethysmograph is reflected in a gradual increase **1378** in detected intensity.

FIG. **14** illustrates the digital signal processing for plethysmograph feature extraction **630** (FIG. **6**). The input **614** is the IR signal output from the demultiplexer **710** (FIG. **7**). This signal is shifted into a first-in, first-out (FIFO) buffer, which allows fixed-length portions of the input signal **614** to be processed for feature extraction. The buffered output signal **1412** is coupled to a shape detector **1420**, slope calculator **1430**, feature width calculator **1440** and a notch locator **1450**, which perform the core feature extraction functions. The shape detector **1420** determines if a particular buffered signal portion **1412** contains specific gross features, such as a peak, a valley, an upward slope, a downward slope, a dicrotic notch or a multiple dicrotic notch. A detected shape output **1422** containing one or more flags indicating the gross feature content of the current signal portion **1412** is coupled to the other feature extraction functions **1430**, **1440**, **1450** and to the waveform quality determination functions **1460**, **1470**, **1480**. A slope calculator **1430** determines the amount of positive or negative slope in the signal portion **1412** if the shape detector output **1422** indicates a slope is present. The output slope value **1432** is coupled to the waveform quality functions **1460**, **1470**, **1480** in addition to the feature extraction output **632**. A feature calculator **1440** quantifies a feature in one or more signal portions **1412** specified by the shape detector **1420**, such as the magnitude, the area under, or the width of a peak or notch. The feature calculator output **1442** is a code indicating the feature and its value, which is coupled to the feature extraction output **632**. A feature locator **1450** quantifies the time of occurrence of one or more features of a signal portion **1412** as specified by the shape detector **1420**. The feature locator output **1452**, which is coupled to the feature extraction output **632**, is a code indicating a feature and an associated code indicating time of occurrence in reference to a particular epoch. The feature locator output **1452** allows a determination of the relative location of plethysmograph features in addition to a phase comparison of plethysmographs derived from two or more tissue sites. Another feature extraction output **634**, which is coupled to the multiple parameter processor **640** (FIG. **6**), provides an indication of waveform quality. Input signals portions **1412** not having either a sharp downward edge **1460**, a symmetrical peak **1470** or a gradual decline **1480** are not processed further.

Multiple Parameter Processor

FIG. **15** illustrates the multiple parameter processing portion **640** (FIG. **6**) of the signal processing. A differencing function **1510** has as inputs a first saturation value, Sp_1O_2, and a second saturation value, Sp_2O_2, **622**. The saturation input values **622** can be arterial and venous saturation values from a single data channel, arterial saturation values from two different data channels or venous saturation values from two different data channels. The differences of the saturation value inputs **622** are provided as an output **1514**, which is coupled to a saturation data memory **1520**. The saturation values **622** are also directly coupled to the saturation data memory **1520**. The memory **1520** stores a record of saturation values, SpO_2, for each channel, delta saturation values, Δsat, for each channel and cross-channel delta saturation values, Δsat_{xy}, as required for a particular application. A flow calcu-

lator **1530** utilizes a plethysmograph input **614** or a bio-impedance probe input **1534** to provide a flow value **1538**, which is also coupled to the saturation data memory **1520**. For example, the flow value **1538** may be a perfusion index, PI, defined as follows:

$$PI = \frac{IR_{max} - IR_{min}}{IR_{DC}} \tag{11}$$

where IR_{max} is the maximum value, IR_{min} is the minimum value, and IR_{DC} is the average value of the IR plethysmograph signal **614** (FIG. **7**).

The saturation data memory **1520** provides a buffered output **1522** that is coupled to a numerical display driver **1540**. The numerical display driver **1540** provides an output **642** to a standard display, such as LED or LCD numerical display modules or a CRT monitor. The memory output **1522** is also coupled to a saturation data analyzer **1530**, one function of which calculates a long-term trend of the values in memory **1520**. For example, the saturation data analyzer may average a saturation value over time, or provide samples of the saturation values taken at regular time intervals. The output **1532** can either be numerical, which is coupled to the numerical display driver **1540**, or graphical, which is coupled to the graphical display driver **1570**. The graphical display driver **1570** provides an output **644** to a standard graphical display device, such as LED or LCD graphical display modules or a CRT monitor.

A pleth data memory **1550** has as inputs the IR plethysmograph signals **614** (FIG. **7**) from each data channel and the associated extracted features **632** (FIG. **14**). The memory **1550** also has an input indicating waveform quality **634** (FIG. **14**). The pleth memory **1550** provides a buffered output **1558** that is coupled to the graphical display driver **1570**, allowing display of the plethysmograph waveforms for each data channel. The memory output **1558** is also coupled to a pleth data analyzer **1560**, one function of which calculates a long-term trend of the plethysmograph and shape parameters in pleth memory **1520**. For example, the pleth data analyzer **1560** may provide an average of particular shape parameters over time. As another example, the pleth data analyzer **1560** may provide a graphic showing an accumulation of many overlaid plethysmographs. The output **1562** can either be numerical, which is coupled to the numerical display driver **1540**, or graphical, which is coupled to the graphical display driver **1570**.

Another function of the saturation data analyzer **1530** and the pleth data analyzer **1560** is to compare oxygen status and plethysmograph parameters derived from multiple sites in order to isolate noise artifacts and to derive a more accurate estimate of these parameters. For example, it is unlikely that motion artifact will affect each peripheral site in the same manner. If the quality input **634** indicates a noisy plethysmograph for one channel during a particular time period, the pleth data analyzer **1560** can exchange this information **1565** with the saturation data analyzer **1530**. The saturation data analyzer **1530** can then ignore the saturation data for that channel for that time period in lieu of saturation data from another channel. In a similar fashion, noisy data from multiple channels can be averaged, correlated or otherwise processed to provide an estimate of Sp_aO_2, Sp_vO_2 or pulse rate, or to provide a plethysmograph that is more accurate than can be derived from a single data channel.

FIG. **16A** illustrates detail of a single-site display screen **180** for the stereo pulse oximeter. The display has a numerical

display portion **1610** controlled by the numerical display driver **1540** (FIG. **15**) and a graphical display portion **1660** controlled by the graphical display driver **1570** (FIG. **15**). The numerical display portion **1610** displays a value for Sp_aO_2 **1620**, Sp_vO_2 **1630** and pulse rate **1640** for a particular tissue site. The graphical display portion **1660** displays a plethysmograph **1662** for the corresponding tissue site, which can be displayed as a single waveform or an accumulated multiple of overlayed waveforms that may reveal a waveform trend. A push button or menu selection allows the user to switch to a display of data from any single one of the multiple tissue sites to which a sensor is attached.

FIG. **16B** illustrates detail of a multi-site display screen **180** for the stereo pulse oximeter. The numerical display portion **1610** displays a value for Sp_aO_2 **1622** and Sp_vO_2 **1632** for a first tissue site. Also displayed is a value for Sp_aO_2 **1624** and Sp_vO_2 **1634** for a second tissue site. In addition, a value for pulse rate **1642** derived from either the first or second tissue site, or both, is displayed. The graphical display portion **1660** displays a first plethysmograph **1664** and a second plethysmograph **1666** corresponding to the first and second tissue sites, respectively. A push button, menu selection allows the user to manually switch between the single site display (FIG. **16A**) and the multi-site display (FIG. **16B**). Also, a triggering event, such as an alarm based on multiple-site oxygen status parameters, causes the display to automatically switch from the single-site display to the multi-site display, enabling the user better view the conditions that caused the triggering event.

One of ordinary skill will appreciate many display screens variations from those shown in FIGS. **16A** and **16B** that are within the scope of this invention. For example, the stereo pulse oximeter could be configured to provide several push button or menu selectable display screens. One display screen might display more than two channels of oxygen status data. Another display screen could display cross-channel parameters such as Δsat_{xy} or a comparison of plethysmograph shape parameters from two channels. One of ordinary skill will also appreciate many variations and modifications of layout and design for the graphical and numerical displays within the scope of this invention.

Stereo Pulse Oximetry Applications

Oxygen Titration

Oxygen is one of the most commonly used drugs in an intensive care unit and is an integral part of all respiratory support. The goal of oxygen therapy is to achieve adequate delivery of oxygen to the tissues without creating oxygen toxicity. Too little oxygen results in organ damage and, in particular, brain damage. Too much oxygen can result in, for example, pulmonary edema and, in neonates, retinopathy of prematurity (ROP). Infants receiving oxygen therapy, in particular, must have inspired oxygen concentration and blood oxygen levels monitored closely.

Oxygen titration in neonates is currently accomplished with either transcutaneous monitoring or monitoring with a conventional pulse oximeter. As mentioned above, transcutaneous monitoring involves the placement of a heated Clark electrode against the skin surface. The electrode is secured to the skin surface with an airtight seal to eliminate contamination by room air gases. The skin surface beneath the electrode is then heated, which opens pre-capillary sphincters allowing localized arteriolar blood flow beneath the sensor. The so-called T_cO_2 value that is measured correlates well with P_aO_2. However, there are several drawbacks to this approach. Because the skin surface must be heated, a fifteen minute elapsed time after application is necessary before stable readings are acquired. Further, the required temperature is 43-45°

C. (110° F.), with an associated risk of burns. In addition, titration is often accomplished by simply maintaining T_cO_2 within acceptable limits for this parameter, e.g. an equivalent P_aO_2 of 50-80 mm Hg for neonates. However, P_aO_2 alone does not provide an indication of balance between inspired oxygen and the rate of tissue oxygen consumption. If the patient is particularly anemic or hypovolemic, has an abnormal hemoglobin, or a small cardiac output, then oxygen delivery may be inadequate even in the presence of a normal P_aO_2. Titration with a conventional pulse oximeter is similarly accomplished by maintaining Sp_aO_2 within acceptable limits, which also fails to consider tissue oxygen consumption.

Oxygen titration can be more adequately monitored with a continuous indication of oxygen consumption, which is equal to oxygen delivery according to Fick's algorithm, as noted above. Further, continuous monitoring of oxygen consumption at a peripheral tissue site, although not necessarily indicative of overall oxygen consumption, may be indicative of an oxygen supply dependency. A measure of peripheral oxygen consumption can be expressed in terms of $\Delta sat = Sp_aO_2 - Sp_vO_2$ and perfusion, which, as noted above, are parameters advantageously provided by the stereo pulse oximeter according to the present invention. Oxygen consumption at a peripheral site is obtained by multiplying the difference between peripheral arterial and venous oxygen content by perfusion at the site.

$$VpO_2 = [O_2 \text{ content (arterial)} - O_2 \text{ content (venous)}]\Phi \qquad (12)$$

where oxygen content is measured in milliliters (ml) of O_2 per deciliters (dl) of blood and Φ denotes perfusion in deciliters per minute. Oxygen content, however, can be expressed in terms of the amount of oxygen bound to the hemoglobin plus the amount of oxygen dissolved in the plasma. The amount of bound oxygen is equal to the hemoglobin concentration, C_{Hb}, in grams per deciliter of blood, times the hemoglobin carrying capacity, which is 1.34 milliliters of O_2 per gram of hemoglobin times the hemoglobin oxygen saturation, SO_2. The amount of dissolved oxygen is simply the partial pressure of oxygen, PO_2, times the O_2 solubility coefficient in blood, which is 0.003 milliliters of O_2 per deciliter. The sum of these two terms yields:

$$O_2 \text{ content} = 1.34 C_{Hb} SO_2 + 0.003 PO_2 \qquad (13)$$

Substituting equation (13) into equation (12) yields the following equation for tissue oxygen consumption:

$$VpO_2 = [1.34 C_{Hb}(Sp_aO_2 - Sp_vO_2) + 0.003(P_aO_2 - P_vO_2)]\Phi \qquad (14)$$

Except when the fractional inspired oxygen, FiO_2, is high, blood plasma plays a minimal role in oxygen delivery. Thus, peripheral oxygen consumption is approximately:

$$VpO_2 = [1.34 C_{Hb}\Delta sat]\Phi \qquad (15)$$

In order to illustrate a schema of oxygen titration, it is convenient to characterize the relationship between oxygen supplied at the airway to oxygen consumed at a peripheral tissue site. Specifically, characterization of the relationship between Δsat, Φ and FiO_2 is useful. Assuming constant oxygen consumption at the tissue site, equation (15) is:

$$\Delta sat\Phi = constant \qquad (16)$$

Equation (16) has a simple analog in electronic circuits, i.e. a variable resistor across a current or voltage source adjusted to maintain constant power. In this analog circuit, the current through the resistor, I, is equivalent to perfusion, the voltage across the resistor, V, is equivalent to Δsat and the constant of

equation (16) is equivalent to the constant power, P, consumed by the resistor. The equation representing this electrical analog is:

$$V \times I = P \qquad (17)$$

FIG. **17A** shows a graph **1701** that depicts a family of curves each corresponding to different values of P in equation (17). The graph **1701** has an x-axis **1710** indicating current, I, and a y-axis **1720** indicating voltage, V. A first curve **1730** shows V versus I for a constant power, P, of 0.5 watts; a second curve **1740** shows V versus I for a constant P of 1 watt; and a third curve **1750** shows V versus I for a constant P of 2 watts. Using the analogy between equations (16) and equation (17), whenever Φ (current) is small, the Δsat (voltage) is large and vice-a-versa. Also, a change in consumption (power) causes a shift in the curve along with a change in its curvature. That is, if the body suddenly changes its metabolic rate at the peripheral tissue site, the curve will accordingly shift up or shift down and will change its shape. Equation (16) and the analogous constant consumption curves of FIG. **17A** assume a supply independent condition, i.e. that peripheral oxygen consumption is satisfied by peripheral oxygen delivery. If the peripheral tissue site is starved for oxygen, then the locus of points for Δsat versus Φ is quite different from a hyperbola The amount of tissue oxygen extraction is at a maximum and is independent of Φ. Accordingly Δsat is at a maximum and independent of Φ. The above analysis provides insight into the relationship between Δsat and Φ. The relationship between Δsat and FiO₂ can also be characterized.

FIG. **17B** shows a graph **1702** of saturation along a y-axis **1760** and fractional inspired oxygen along an x-axis **1770**. A curve of Sp$_a$O₂ **1780** and a curve of Sp$_a$O₂ **1790** are depicted versus FiO₂. The difference between these curves **1780**, **1790** yields Δsat **1785** versus FiO₂. When FiO₂ is zero **1772**, oxygen saturation and, hence, both Sp$_a$O₂ **1780** and Sp$_v$O₂ **1790** are zero. As FiO₂ is increased, Sp$_a$O₂ **1780** also increases until virtually reaching 100 percent saturation **1762**. As FiO₂ increases further, Sp$_a$O₂ **1780** stays at virtually 100 percent saturation **1762**. As FiO₂ is increased from zero **1772**, Sp$_v$O₂ **1790** also increases. In this low FiO₂ region **1774**, the peripheral tissue site is supply dependent and Δsat **1785** also increases. At a certain point, the tissue site oxygen demand is met by supply. In this supply independent region **1776**, oxygen consumption is constant and equation (16) is valid. Also, Δsat **1785** is at a constant maximum, which is a function of the metabolism at the tissue site. As FiO₂ increases further, eventually the partial pressure of oxygen becomes significant and the second term of equation (14) must be considered. In this high FiO₂ region **1778**, Δsat **1785** decreases because some of the tissue oxygen consumption is supplied by oxygen dissolved in the plasma.

FIG. **17C** shows a graph **1704** of saturation difference along a y-axis **1764** and fractional inspired oxygen along an x-axis **1770**. A curve of Δsat **1786** is depicted versus FiO₂, corresponding to the region Δsat **1785** depicted in FIG. **17B**. The curve **1786** has a first deflection point **1766** occurring at the transition between the low FiO₂ region **1774** (FIG. **17B**) and the supply independent region **1776** (FIG. **17B**). The curve **1786** also has a second deflection point **1768** occurring at the transition between the supply independent region **1776** (FIG. **17B**) and the high FiO₂ region **1778** (FIG. **17B**). The curve **1786** illustrates how the trend for Δsat, as measured by the stereo pulse oximeter, can be used to accurately titrate oxygen. The goal of oxygen titration is to supply sufficient oxygen to supply tissue demand and avoid unnecessarily high amounts of FiO₂. Thus, the Δsat parameter should be monitored so that FiO₂ is adjusted between the two deflection

points **1766**, **1768**. For neonates, FiO₂ should be adjusted just beyond the first deflection point **1766**. For adults, FiO₂ should be adjusted just before the second deflection point **1768**.

FIG. **18** illustrates a graph having a three-dimensional surface **1800** generally depicting the relationship between Δsat, Φ and FiO₂ from the combined graphs of FIGS. **17A** and **17C**. The graph has an x-axis **1810** showing FiO₂, a y-axis **1820** showing Φ and a z-axis **1830** showing Δsat. The surface **1800** has a supply dependent region **1840**, a perfusion-limited region **1850**, a constant consumption region **1860** and a plasma dependent region **1870**. The surface describes the oxygen status of a peripheral tissue site. The supply dependent region **1840** corresponds to the low FiO₂ region **1774** (FIG. **17B**) described above. That is, inspired oxygen into the lungs is so low that, at the tissue site, oxygen extraction by the tissues is limited by oxygen delivery, and Δsat falls rapidly as FiO₂ is reduced. The perfusion-limited region **1850** along the x-axis **1810** represents a low perfusion state where equation (16) is not valid. That is, perfusion at the tissue site is so low that oxygen extraction by the tissues is at a maximum, and, hence, Δsat is at a maximum and is independent of FiO₂. A cross-section of the surface taken parallel to the y-axis **1820** yields a hyperbole-shaped constant consumption region **1860**, consistent with the constant metabolic rate curves illustrated above with respect to FIG. **17A**. The plasma dependent region **1870** corresponds to the high FiO₂ region **1778** (FIG. **17B**) described above. That is, inspired oxygen into the lungs is so high that the tissue site is partially dependent on oxygen dissolved in the plasma The surface **1800** illustrates that perfusion should be monitored simultaneously with Δsat to avoid the perfusion-limited region **1850**, where Δsat is an unresponsive indicator of FiO₂, and to avoid misinterpreting hyperbolic changes in Δsat that result from changes in perfusion.

Persistent Pulmonary Hypertension in Neonates

FIG. **19** illustrates the heart/lung circulation of a hypertensive neonate. Persistent Pulmonary Hypertension in Neonates (PPHN) is a neonatal condition with persistent elevation of pulmonary vascular resistance and pulmonary artery pressure. Shown is a neonatal heart **1902** and a portion of a neonatal lung **1904**. The pulmonary artery **1910** that normally feeds oxygen depleted "blue" blood from the right ventricle **1920** to the lung **1904** is constricted. The back pressure from the constricted artery **1910** results in a right-to-left shunting of this oxygen depleted blood through the ductus arteriosus **1930**, causing it to mix with oxygen rich "red" blood flowing through the descending aorta **1940**. PPHN treatment options include vasodilators, such as nitric oxide (NO). Inhaled exogenous NO causes a dose-dependent decrease in pulmonary artery pressure and pulmonary vascular resistance, as well as a parallel increase in pulmonary blood flow, without affecting systemic arterial pressure. However, the response to NO therapy is a function of the cause of the PPHN as well as the time elapsed before initiation of therapy. Potential toxic effects of NO dictate the proper titration of NO gas. Too little NO may not effectively relieve pulmonary hypertension, and too much NO may cause cellular injury or toxicity. NO therapy is currently monitored using intermittent ultrasound imaging and/or in vitro blood gas measurements. The drawbacks to these techniques are noncontinuous monitoring and disturbances to the neonate that can exacerbate or not reflect the hypertension in the non-disturbed state.

The stereo pulse oximeter according to the present invention allows noninvasive, continuous monitoring of a neonate for detection and managed treatment of PPHN that does not disturb the patient. A right hand sensor **130** (FIG. **1**) provides arterial oxygen saturation and a plethysmograph for blood circulating from the left ventricle **1950** through the innomi-

nate artery **1960**, which supplies the right subclavian artery. Because the innominate artery **1960** is upstream from the shunt at the ductus arteriosus **1930**, the oxygen saturation value and plethysmograph waveform obtained from the right hand are relatively unaffected by the shunt and serve as a baseline or reference for comparison with readings from other tissue sites. Alternatively, a reference sensor can be placed on a facial site, such as an ear, the nose or the lips. These sites provide arterial oxygen saturation and a plethysmograph for blood circulating from the left ventricle **1950** to the innominate artery **1960**, which supplies the right common carotid artery (not shown), or to the left common carotid artery **1965**.

A foot sensor **120** (FIG. **1**) provides oxygen status for blood supplied from the descending aorta **1940**. The shunt **1930** affects both the oxygen saturation and the blood flow in the descending aorta **1940**. As stated above, the shunt **1930** causes oxygen-depleted blood to be mixed with oxygen-rich blood in the descending aorta **1940**. Because the descending aorta **1940** supplies blood to the legs, the oxygen saturation readings at the foot will be lowered accordingly. The PPHN condition, therefore, is manifested as a higher arterial oxygen saturation at the right hand reference site and a lower saturation at the foot site.

The shunt also allows a transitory left to right flow during systole, which distends the main pulmonary artery **1980** as the result of the blood flow pressure at one end from the right ventricle and at the other end from the aortic arch **1990**. A left-to-right flow through the shunt **1930** into the distended artery **1980** alters the flow in the descending aorta **1940** and, as a result, the plethysmograph features measured at the foot. The PPHN condition, therefore, also is manifested as a plethysmograph with a narrow peak and possibly a well-defined dicrotic notch at the left hand baseline site and a broadened peak and possibly no notch at the foot site.

An optional left hand sensor **110** (FIG. **1**) provides oxygen status for blood circulating from the left ventricle through the left subclavian artery **1970** that supplies the left arm. Because the left subclavian artery **1970** is nearer the shunt **1930** than the further upstream innominate artery **1960**, it may experience some mixing of deoxygenated blood and an alteration in flow due to the shunt **1930**. The PPHN condition, therefore, may also be manifested as a reduced saturation and an altered plethysmograph waveform at the left hand site as compared with the right hand baseline site, although to a lesser degree than with a foot site. Thus, the PPHN condition can be detected and its treatment monitored from Δsat and plethysmograph morphology comparisons between a right hand baseline sensor site and one or more other sites, such as the left hand or foot.

Patent Ductus Arteriosus

FIG. **20** illustrates the fetal heart/lung circulation. Shown is a fetal heart **2002** and a portion of a fetal lung **2004**. The lung **2004** is non-functional and fluid-filled. Instead, oxygenated blood is supplied to the fetus from gas-exchange in the placenta with the mother's blood supply. Specifically, oxygenated blood flows from the placenta, through the umbilical vein **2006** and into the right atrium **2022**. There, it flows via the foramen **2024** into the left atrium **2052**, where it is pumped into the left ventricle **2050** and then into the aortic trunk **2092**. Also, oxygenated blood is pumped from the right atrium **2022** into the right ventricle **2020** and directly into the descending aorta **2040** via the main pulmonary artery **2080** and the ductus arteriosus **2030**. Normally, the ductus arteriosus **2030** is only open (patent) during fetal life and the first 12 to 24 hours of life in term infants. The purpose of the ductus arteriosus **2030**

is to shunt blood pumped by the right ventricle **2020** past the constricted pulmonary circulation **2010** and into the aorta **2040**.

FIG. **21** illustrates a neonatal heart **2002** with a patent ductus arteriosus **2030**. The ductus arteriosus frequently fails to close in premature infants, allowing left-to-right shunting, i.e. oxygenated "red" blood flows from the aorta **2040** to the now unconstricted pulmonary artery **2010** and recirculates through the lungs **2004**. A persistent patent ductus arteriosus (PDA) results in pulmonary hyperperfusion and an enlarged right ventricle **2020**, which leads to a variety of abnormal respiratory, cardiac and genitourinary symptoms. Current PDA diagnosis involves physical examination, chest x-ray, blood gas analysis, echocardiogram, or a combination of the above. For example, large PDAs may be associated with a soft, long, low-frequency murmur detectable with a stethoscope. As another example, two-dimensional, color Doppler echocardiography may show a retrograde flow from the ductus arteriosus **2030** into the main pulmonary artery **2080**. Once a problematic PDA is detected, closure can be effected medically with indomethacin or ibuprofen or surgically by ligation. Multiple doses of indomethacin are commonplace but can still result in patency, demanding ligation. A drawback to current diagnostic techniques is that clinical symptoms of a PDA can vary on an hourly basis, requiring extended and inherently intermittent testing.

The stereo pulse oximeter according to the present invention allows for continuous evaluation of PDA symptoms using non-invasive techniques. A right hand sensor **130** (FIG. **1**) provides arterial oxygen saturation and a plethysmograph for blood circulating from the left ventricle **2050** through the innominate artery **2160**, which supplies the right subclavian artery leading to the right arm. Because the innominate artery **2160** is upstream from the shunt at the ductus arteriosus **2030**, the oxygen saturation value and plethysmograph waveform obtained from the right hand are relatively unaffected by the shunt and serve as a baseline for comparison with readings from other tissue sites.

A foot sensor **120** (FIG. **1**) provides oxygen status for blood supplied from the descending aorta **2040**. Unlike a PPHN condition, the shunt **2030** does not affect oxygen saturation in the descending aorta **2040**, because the relatively low pressure in the pulmonary artery **2010** does not allow a mixing of deoxygenated blood into the relatively high pressure flow of oxygenated blood in the aorta **2040**. However, like a PPHN condition, the shunt **2030** does affect the aortic flow. In particular, the shunt allows a transitory left-to-right flow during systole from the high pressure aorta **2040** to the low pressure pulmonary circulation **2010**. This left-to-right flow through the shunt **1930** alters the flow in the descending aorta **1940** and, as a result, the plethysmograph features measured at the foot. The PDA condition, therefore, is manifested as a normal plethysmograph with a characteristically narrow peak and well-defined dicrotic notch at the right-hand baseline site compared with a damped plethysmograph with a broadened peak and reduced or missing notch at the foot site. Further, the foot site waveform is phase shifted from the baseline waveform. These plethysmograph differences are accompanied by comparable arterial oxygen saturation values between the right-hand site and the foot site.

An optional left hand sensor **110** (FIG. **1**) provides oxygen status for blood circulating from the left ventricle through the left subclavian artery **2170** that supplies the left arm. Because the left subclavian artery **2170** is nearer the shunt **2030** than the further upstream innominate artery **2160**, it may experience some alteration in flow due to the shunt **2030**. The PDA condition, therefore, may also be manifested as an altered

plethysmograph waveform at a left hand site as compared with the right hand baseline site, although to a lesser degree than with a foot site. Thus, the PDA condition can be detected and its treatment monitored from $\Delta sat_{xy} \approx 0$ and plethysmograph morphology and phase comparisons between a right hand baseline sensor site and one or more other sites, such as the left hand or foot. One of ordinary skill will recognize that multiple site comparisons using the stereo pulse oximeter of the current invention may also be used to detect other cardiac abnormalities that cause mixing of oxygenated and deoxygenated blood, such as a ventricular hole or a patent foramen. Further, abnormal mixing of oxygenated and deoxygenated blood may also be manifested in measurements provided by the stereo oximeters other than Δsat_{xy} and $-\Delta pleth_{xy}$ as described above. For example, an inversion in Δsat at a particular tissue site, i.e., Sp_vO_2 being larger than Sp_aO_2 at that site, would indicate such an abnormal condition.

Aortic Coarctation

Coarctation of the aorta is a congenital cardiac anomaly in which obstruction or narrowing occurs in the distal aortic arch or proximal descending aorta. It occurs as either an isolated lesion or coexisting with a variety of other congenital cardiac anomalies, such as a PDA. If the constriction is preductal, lower-trunk blood flow is supplied predominantly by the right ventricle via the ductus arteriosus, and cyanosis, i.e. poorly oxygenated blood, is present distal to the coarctation. This can be detected by the stereo pulse oximeter from a comparison of Sp_aO_2 between an upper body and a lower body site. If the constriction is postductal, blood supply to the lower trunk is supplied via the ascending aorta Differential plethysmographs between the upper and lower extremities may not exist if the ductus is widely patent. If the ductus closes, however, this condition can be detected by the stereo pulse oximeter as a reduced amplitude and phase delay between the plethysmographs measured at a lower body site with respect to an upper body site.

The stereo pulse oximeter has been disclosed in detail in connection with various embodiments of the present invention. These embodiments are disclosed by way of examples only and are not to limit the scope of the present invention, which is defined by the claims that follow. One of ordinary skill in the art will appreciate many variations and modifications within the scope of this invention.

What is claimed is:

1. A patient monitor capable of measuring at least two physiological parameters, the patient monitor comprising:
   a processor configured to receive sensor data and determine a measured value of a first physiological parameter and a measured value of a second physiological parameter of body tissue of a monitored patient,
   wherein the processor is further configured to cause a display to display the measured value of the first physiological parameter in a common portion of the display or display the measured value of the second physiological parameter in the common portion of the display, and
   wherein the processor further causes the common portion of the display to change to displaying, at least, the other of the measured values based on an occurrence of a triggering event.

2. The patient monitor of claim 1, wherein the triggering event comprises an alarm condition.

3. The patient monitor of claim 1, wherein the common portion of the display is configured to display the first physiological parameter and the second physiological parameter after the occurrence of the triggering event.

4. The patient monitor of claim 1, wherein activation of a user input causes the common display area to change from

displaying one of the measured values of the first or second physiological parameter to displaying the other of the measured value of the first or second physiological parameter.

5. The patient monitor of claim 1, wherein the common display area is configured to default to displaying one of the measured values of the first or second physiological parameters.

6. The patient monitor of claim 1, wherein the measured value of the first physiological parameter comprises an indication of arterial oxygen saturation.

7. The patient monitor of claim 1, wherein the measured value of the first physiological parameter comprises an indication of venous oxygen saturation.

8. The patient monitor of claim 1, wherein the measured value of the first physiological parameter comprises a plethysmograph.

9. The patient monitor of claim 1, wherein an aspect of the display changes based on the occurrence of the triggering event, wherein the aspect that changes comprises the positioning of the first or second physiological parameter within the common portion of the display.

10. A method of displaying two physiological parameter measurements using a display location of a display of a patient monitoring device, the method comprising:
    using a processor, receiving sensor data and determining a measured value of a first physiological parameter and a measured value of a second physiological parameter of body tissue of a monitored patient;
    displaying the measured value of the first physiological parameter in a display location of an electronic display; and
    changing the display of the measured value of the first physiological parameter to display, at least, the measured value of the second physiological parameter in the display location when a change in the measurement of the second physiological parameter causes a triggering event.

11. The method of claim 10, wherein the triggering event comprises an alarm condition.

12. The method of claim 10, wherein the measured value of the first physiological parameter comprises a noninvasively measured value.

13. The method of claim 10, wherein the measured value of the first physiological parameter comprises an indication of oxygen saturation.

14. A patient monitor capable of determining a plurality of physiological parameters from an output signal of a light sensitive detector capable of detecting light attenuated by body tissue, the patient monitor comprising:
    a processor configured to cause a display to display a measured value of a first blood parameter of body tissue of a monitored patient or display a measured value of a second blood parameter of the body tissue; and
    a user input button, the activation of which causes the display to change from displaying the measured value of the first blood parameter to displaying, at least, the measured value of the second blood parameter, wherein the display is also configured to change from displaying the measured value of the first blood parameter to displaying, at least, the measured value of the second blood parameter when the second blood parameter passes an alarm threshold,
    wherein the measured values of the first and second blood parameters are determined by the processor using an output signal of a noninvasive light sensitive detector capable of detecting light attenuated by the body tissue.

15. The patient monitor of claim **14** wherein the display shifts a positioning of the display of the second blood parameter with respect to a positioning of the display of the first blood parameter.

16. The patient monitor of claim **14**, further comprising an alarm corresponding to either of the measured values of the first and second blood parameters.

17. The patient monitor of claim **14**, wherein the first blood parameter comprises oxygen saturation.

* * * * *

UNITED STATES PATENT AND TRADEMARK OFFICE
CERTIFICATE OF CORRECTION

PATENT NO.   : 8,721,541 B2   Page 1 of 1
APPLICATION NO. : 13/745590
DATED   : May 13, 2014
INVENTOR(S)   : Ammar Al-Ali et al.

It is certified that error appears in the above-identified patent and that said Letters Patent is hereby corrected as shown below:

Title Page

In column 1 (page 5, item 56) at line 27, Under Other Publications, change "Phlips'" to --Philips'--.

In column 2 (page 5, item 56) at line 27, Under Other Publications, change "Noenates\"," to --Neonates\",--.

In the Specification

In column 1 at line 58, Change "intervascular" to --intravascular--.

In column 12 at line 65, Change "-μ_b" to --.μ_b--.

In column 12 at line 66, Change "-μ_t" to --.μ_t--.

In column 13 at line 1, Change "-μt," to --.μt,--.

In column 13 at lines 43-44, Change "RD(ω)/ RD(ω)." to --RD(ω)/ IR(ω).--.

In column 23 at line 14, Change "-$\Delta pleth_{xy}$" to --.$\Delta pleth_{xy}$--.

Signed and Sealed this
Eleventh Day of November, 2014

Michelle K. Lee
Deputy Director of the United States Patent and Trademark Office

专利名称(译)	生理监测		
公开(公告)号	US8721541	公开(公告)日	2014-05-13
申请号	US13/745590	申请日	2013-01-18
[标]申请(专利权)人(译)	梅西莫股份有限公司		
当前申请(专利权)人(译)	Masimo公司		
[标]发明人	AL ALI AMMAR DIAB MOHAMED K KIANI MASSI E KOPOTIC ROBERT JAMES TOBLER DAVID		
发明人	AL-ALI, AMMAR DIAB, MOHAMED K. KIANI, MASSI E. KOPOTIC, ROBERT JAMES TOBLER, DAVID		
IPC分类号	A61M16/00 A61B5/1455 A61B5/00 A61B5/024 A61B5/145		
CPC分类号	A61M16/00 A61B5/14551 A61B5/6829 A61B5/746 A61B5/1459 A61B5/6814 A61B5/6838 A61B5/742 A61M2230/205 A61B5/02416 A61B5/6826 A61B5/0205 A61B5/6819 A61B5/6825 A61B5/6815 A61M16/021		
优先权	11/104720 2010-07-20 US 10/668487 2005-05-24 US 10/026013 2004-03-30 US 09/323176 2001-12-25 US 60/087802 1998-06-03 US		
其他公开文献	US20130197330A1		
外部链接	Espacenet USPTO		

摘要(译)

患者监测器具有多个适于附着到活体的组织部位的传感器。传感器产生传感器信号，其在组织部位内的脉动血液衰减之后响应于至少两个波长的光辐射。